Title

Modeling Ammonia and Its Uptake by Secondary Organic Aerosol Over China

Journal

Journal of Geophysical Research: Atmospheres, 126(7)

ISSN

2169-897X

Authors

Wu, Kai
Zhu, Shupeng
Liu, Yiming
et al.

Publication Date

2021-04-16

DOI

10.1029/2020jd034109

Peer reviewed

Modeling Ammonia and Its Uptake by Secondary Organic Aerosol over China

Kai Wu[1,2], Shupeng Zhu[2,3*], Yiming Liu[4,5], Haolin Wang[4,5], Xianyu Yang[6], Lei Liu[7], Donald Dabdub[3], Christopher D. Cappa[8*]

[1] Department of Land, Air, and Water Resources, University of California, Davis, CA, USA.

[2] Advanced Power and Energy Program, University of California, Irvine, CA, USA.

[3] Computational Environmental Sciences Laboratory, Department of Mechanical and Aerospace Engineering, University of California, Irvine, CA, USA.

[4] School of Atmospheric Sciences, Sun Yat-sen University, Zhuhai, Guangdong, China

[5] Guangdong Provincial Observation and Research Station for Climate Environment and Air Quality Change in the Pearl River Estuary, Key Laboratory of Tropical Atmosphere-Ocean System, Ministry of Education, Southern Marine Science and Engineering Guangdong Laboratory (Zhuhai), Zhuhai, China.

[6] Plateau Atmosphere and Environment Key Laboratory of Sichuan Province, School of Atmospheric Sciences, Chengdu University of Information Technology, Chengdu, China.

[7] College of Earth and Environmental Sciences, Lanzhou University, Lanzhou, China.

[8] Department of Civil and Environmental Engineering, University of California, Davis, CA, USA

Corresponding author: S. Zhu (sz@apep.uci.edu), C. D. Cappa (cdcappa@ucdavis.edu)

Key Points:

(I) Impacts of ammonia uptake mechanism on particle matters over China are presented and analyzed.

(II) The reduction of gas-phase NH_3 engenders a decrease of ammonium nitrate but has little impact on the ammonium sulfate concentration.

(III) The inclusion of ammonia uptake mechanism shows moderate changes in aerosol acidity and small effects on SOA formation.

Abstract

Atmospheric ammonia (NH_3) can affect nitrogen deposition, particle acidity, and gas-particle partitioning. Although the inorganic chemistry of NH_3 in fine particulate ($PM_{2.5}$) formation are well-constrained, the understanding of interactions between NH_3 and secondary organic aerosol (SOA) are rather insufficient until recently. Laboratory studies indicate that NH_3 molecule can react with SOA then forms nitrogen-containing organic compounds (NOCs), which can further react to form heterocyclic organic compounds. In this study, we use a modified version of the CMAQ model to simulate the potential importance of the SOA-ammonia uptake mechanism on air quality over China in summer and winter 2017, considering a range of assumed NH_3 uptake coefficients (10^{-3}-10^{-5}). Our results show that uptake of NH_3 by SOA leads to a decrease in gas-phase NH_3 mixing ratio, by as much as 27.5% and 19.0% for the highest uptake coefficient scenario (10^{-3}) in summer and winter, respectively. The largest reduction of ammonia occurs over the Sichuan Basin and the North China Plain. The reduction of gas-phase NH_3 engenders a decrease of ammonium nitrate, by up to 30%, but has little impact on the ammonium sulfate concentration. Uptake of NH_3 does not significantly affect SOA concentrations owing to overall moderate changes in aerosol acidity, and thus small effects on SOA formation from isoprene. Altogether, NH_3 uptake led to a reduction in the average $PM_{2.5}$ concentration up to 8.9% and 8.7% for the highest uptake coefficient (10^{-3}) in summer and winter, respectively. These results highlight the need for better constraints on the NH_3-SOA interactions.

Index terms and keywords: ammonia uptake, particle matter, heterogeneous chemistry, SOA, CMAQ

1 Introduction

As the most abundant alkaline gas in the atmosphere, ammonia (NH_3) plays an important role in atmospheric chemistry (Behera et al., 2013; Heald et al., 2012). According to L. Zhu et al. (2015), NH_3 emissions from anthropogenic sources have become a major environmental concern around the world. Ammonia affects air quality and regional climate change through its role in the formation and composition of tropospheric aerosols (Reiss et al., 2007). The aerosol-phase products of NH_3, including ammonium nitrate and ammonium sulfate, make up a large fraction of fine particulate matter (Jimenez et al., 2009). Moreover, ammonia also influences aerosol pH and total reactive nitrogen deposition (Guo et al., 2018; Li et al., 2016; Weber et al., 2016).

Fertilizer applications associated with agricultural activities and livestock operations are the major sources of NH_3 emissions to the atmosphere. NH_3 emissions in China have nearly reached 10.0 million tons annually owing to the recent ramp-up of intensive agricultural activities and livestock operations, significantly exceeding the NH_3 emissions in the European Union (3.7 million tons) and the United States (3.9 million tons) (Paulot et al., 2014; L. Zhang et al., 2018). Recent studies have suggested that the atmospheric NH_3 concentrations in China has increased significantly between 2008 and 2016 based on satellite and surface NH_3 observations (S. Chen et al., 2020; L. Liu et al., 2017). Furthermore, the ammonia-rich environment in China is expected to continue since the emissions of its primary neutralizer (SO_2 and NO_x) has been dropping rapidly due to more stringent regulation in recent years, while the NH_3 emissions have not been regulated by the Chinese government (Pan et al., 2018).

Sulfate (SO_4^{2-}), nitrate (NO_3^-) and ammonium (NH_4^+) are the main secondary inorganic aerosol (SIA) components in particulate matter (PM), mainly existing in forms as ammonium sulfate and ammonium nitrate. In the presence of HNO_3 and H_2SO_4, NH_3 is first neutralized by the stronger acid H_2SO_4 to form ammonium sulfate ($(NH_4)_2SO_4$) or ammonium bisulfate (NH_4HSO_4) in particulate phase (Baek et al., 2004). The remaining NH_3 reacts with HNO_3 to form NH_4NO_3 in particulate phase (Walters et al., 2019). The formation of ammonium nitrate and ammonium sulfate in the atmosphere are reasonably well understood. In contrast, the role of NH_3 on the formation, chemical composition, and optical properties of organic aerosol, and especially secondary organic aerosol, is poorly established and has received little attention in air quality models. However, laboratory evidence has emerged in recent years offering new clues for understanding the interactions between NH_3 and SOA. Montoya-Aguilera et al. (2018) summarized laboratory findings of how ammonia can affect SOA formation and properties. In general, ammonia can react with SOA compounds heterogeneously via two chemical pathways. It can react with organic acids to form ammonium salts or react with certain carbonyl compounds to form heterocyclic nitrogen-containing organic compounds (NOCs). In addition, observations suggest that ammonia actively participates in SOA formation and leads to chemical compounds in SOA that have unique optical properties (Updyke et al., 2012). While these processes remain uncertain, it is nonetheless important to assess the potential influence of ammonia-SOA interactions on atmospheric SOA, SIA, and ammonia concentrations. Focusing on the United States, S. Zhu et al. (2018) included heterogeneous NH_3 uptake by SOA in an air quality model.

Their results suggest that ammonia uptake may substantially decrease atmospheric ammonia concentrations, thus indirectly decreasing the formation of SIA, and also increase SOA concentrations. However, to our knowledge, there has been no consideration of ammonia-SOA interactions in other locations. Given the large NH_3 emissions in China, coupled with the substantial reduction of SO_2 and NO_x emissions since 2011, ammonia-SOA interactions may play an important role in determining air quality over China.

In this study, we consider the impact of heterogeneous ammonia uptake onto SOA on surface-level atmospheric NH_3 mixing ratio, SOA, SIA, and $PM_{2.5}$ concentrations over mainland China using the U.S. EPA Community Multiscale Air Quality (CMAQ) model (Byun & Schere, 2006). We used the framework developed by S. Zhu et al. (2018), which treats ammonia uptake onto SOA as an irreversible first-order loss process, and consider the importance of this process as a function of the assumed reactive uptake coefficient. The objective of this study is to understand how the inclusion of irreversible NH_3 uptake to SOA affects SOA and SIA concentrations and aerosol acidity in China. Section 2 introduces the updated ammonia uptake module and configuration of model simulations. Section 3 presents the model performance evaluation against surface observations. The simulation results under different uptake coefficient scenarios are analyzed in Section 4.

2 Methodology

2.1 WRF-CMAQ model

In this study, there are eight simulation cases conducted including the base case for the winter (29 December, 2016 to 28 February, 2017), the base case for the summer (28 June, 2017 to 31 August 2017), and three cases under different NH_3 uptake coefficients for each season. To minimize initial-condition influence, the first 3 days in all cases were treated as spin up time and were not analyzed in this study. Meteorological fields are simulated by the Weather Research and Forecasting (WRFv3.9.1) model (Skamarock et al., 2008). The model domain covers the whole of China with horizontal resolution of 27 km, as shown in Figure 1. Model configurations for the WRF-CMAQ modeling system are summarized in Table 1 and the provinces in China categorized by different regions are shown in Table 2 and Figure S1. The initial and boundary conditions for the WRF simulation were obtained from the National Centers for Environmental

Prediction (NCEP) Final (FNL) 1.0° × 1.0° reanalysis data (http://dss.ucar.edu/datasets/ds083.2/). CMAQ v5.2 was used to simulate air pollutants. The initial and boundary conditions for the CMAQ simulations were taken from default CMAQ profiles provided with the northern hemispheric CMAQ results. The Carbon-Bond chemical reaction mechanism (CB06) and a modified version of the Aerosol 06 (AERO6) mechanism, to account for NH_3 uptake, were applied in the CMAQ model. We used the Multi-resolution Emission Inventory for China (MEIC, available at http://meicmodel.org/, last accessed:14th Febrary, 2021) in 2016 to provide the anthropogenic emissions of air pollutants, with a grid resolution of 0.25°×0.25° (Zheng et al., 2018). The biogenic emissions are estimated by Model of Emissions of Gases and Aerosols from Nature (MEGAN) version 2.1 (Guenther et al., 2012).

In this study, the AERO6 module in CMAQ was modified to include the process of heterogeneous uptake of NH_3 by SOA. In AERO6, particles are divided into three log-normal modes based on their size distributions: the Aitken mode (<0.1 μm), the accumulation mode (0.1 to 2.5 μm), and the coarse mode (size between 2.5 to 10 μm) (Binkowski & Roselle, 2003). The particles are assumed to be internally mixed in each mode. In the CMAQ AERO6 module, three integral properties of the size distribution are calculated for mode *j*: the total particle number concentration (N_j), the total surface area concentration (S_j), and the total mass concentration (m_{ij}) of each individual chemical component *i*. The surface area concentration of SOA (S_{SOA}) can be formulated by equation (1) (we assume a uniform density across different chemical components and don't consider the SOA hygroscopic growth in model simulations):

$$S_{SOA} = \sum_{j=1}^{x} \left(S_j \times \frac{\sum_{i=1}^{y} m_{ij}}{\sum_{k=1}^{z} m_{ij}} \right) \quad (1)$$

In equation (1), *x*, *y*, and *z* represent the total number of modes that contain SOA species, the total number of SOA species in mode *j* and the total number of aerosol species in mode *j*, respectively. Because SOA species only exist in the Aitken mode and the accumulation mode, the value of x is setting to 2. Then the first-order rate of NH_3 uptake is calculated by equation (2):

$$k = \gamma \times \frac{v_{NH_3} \times s_{SOA}}{4} \quad (2)$$

In equation (2), γ represents the uptake coefficient for ammonia and v_{NH3} represents the average speed of NH_3 molecules under the condition of 298 K. The first-order rate constant of NH_3 uptake in each grid cell is calculated by using above equations and then multiplied by the NH_3 concentration to determine the NH_3 taken up by SOA. The parameterization used in this study assumed that one NH_3 molecule that reacts with SOA forms nitrogen-containing organic compounds (NOCs), which can further react to form heterocyclic organic compounds with two H_2O molecules as the by-product. The reaction of NH_3 and formation of NOC products generally leads to only small direct changes in the SOA mass concentration given the much larger molecular weight of typical SOA compounds, close to 200 g mol^{-1}, compared to NH_3 (17 g mol^{-1}), and the offsetting loss of two H_2O molecules (The change of SOA mass concentration is $2 \times 18 - 17 = 19$ g mol^{-1}). Thus, we could reasonably neglect the mass loss in the particle organic matters directly due to the implementation of NH_3 uptake. However, assuming that the aerosols have a single phase for both organic and inorganic constituents, irreversible NH_3 uptake by SOA can indirectly influence the concentration of SIA and the SOA mass concentration by altering the particle acidity, which can be attributed to the change of acid-catalyzed heterogeneous reactions. More details about the parameterization of NH_3 uptake can be found in S. Zhu et al. (2018). The rate of NH_3 uptake to SOA depends on the assumed chemical uptake coefficient (γ) of ammonia by all SOA species, which is not especially well established. Based on chamber experiments, Y. Liu et al. (2015) reported that ammonia uptake coefficients (γ) are with a range of 10^{-5} to 10^{-2}, whereas our initial modeling result for the $\gamma = 10^{-2}$ scenario leads to extremely low NH_3 mixing ratio which indicates that unrealistic amount of NH_3 taken up by SOA. Besides, experiments results in Y. Liu et al. (2015) show that less than 10 % of SOA molecules can react with NH_3 to form NOCs and the largest uptake coefficient was observed at the initial time of reactions then significantly decreased. Thus, ammonia uptake coefficients with $\gamma = 10^{-3}$ may be a more reasonable upper limit value for model simulations rather than $\gamma = 10^{-2}$. Based on the discussion above, four simulations were performed for each period to investigate the sensitivity of NH_3 removal to changes in the uptake coefficient: (a) base case without NH_3 uptake to SOA, (b) NH_3 uptake coefficient of $\gamma = 10^{-3}$, (c) NH_3 uptake coefficient of $\gamma = 10^{-4}$, and (d) NH_3 uptake coefficient of $\gamma = 10^{-5}$.

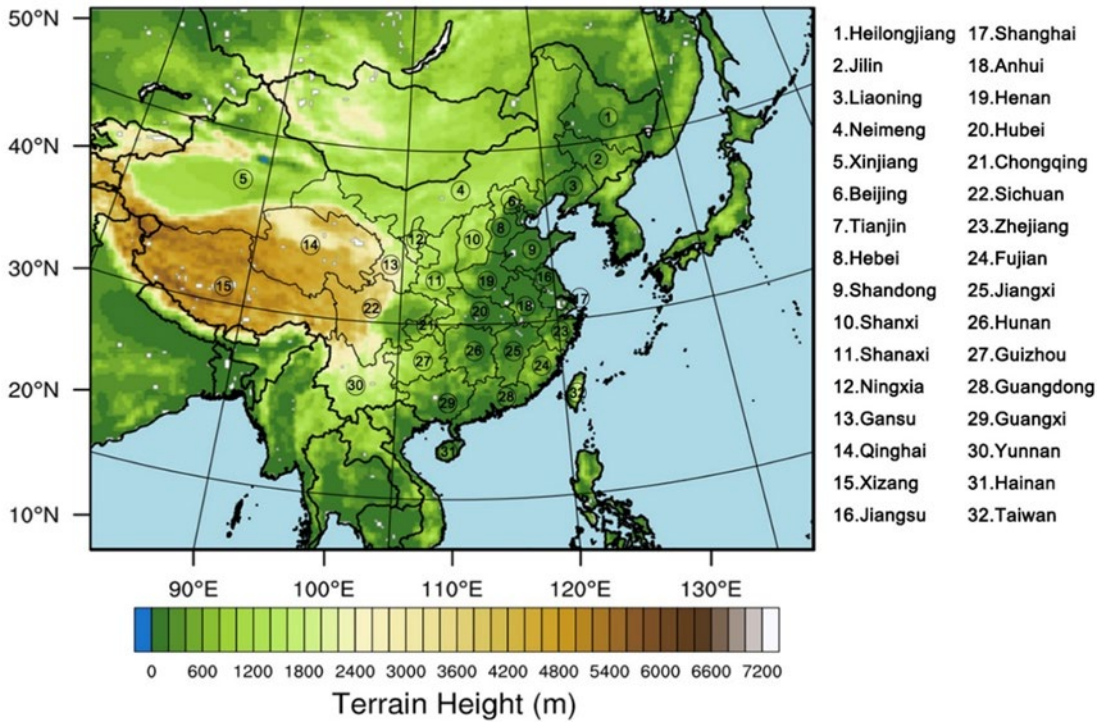

171

172 **Figure 1.** Map showing the simulation domain.

173 **Table 1.** Configuration of the WRF-CMAQ modeling system.

WRF/MCIP			
Version	ARW v3.9.1	**Shortwave radiation**	RRTMG scheme
Horizontal resolution	27km × 27km	**Longwave radiation**	RRTMG scheme
		Surface layer physics	Noah LSM scheme
Vertical layers	30 layers	**Microphysics Cumulus parameterization**	Morrison
Initial condition	NCEP-FNL		Kain-Fritsch scheme
Boundary condition			
PBL scheme	YSU scheme		
CMAQ			
Version	v5.2	**Biogenic Emission**	MEGAN v2.1
Horizontal resolution	Same as WRF	**Anthropogenic emission**	MEIC 2016
Initial condition	Default	**Aerosol module**	AERO06
Boundary condition	Default	**Gas-phase mechanism**	CB06

Table 2. List of the provinces in China categorized by different regions.

Region	Province list
North China Plain	Beijing, Hebei, Tianjin
Yangtze River Delta	Zhejiang, Shanghai, Jiangsu
Pearl River Delta	Guangdong
Central China	Shanxi, Henan, Anhui, Hubei, Hunan, Jiangxi
Sichuan Basin	Sichuan, Chongqing
Northeastern China	Jilin, Heilongjiang, Liaoning
Western China	Xinjiang, Qinghai, Ningxia, Tibet, Guizhou

2.2 Statistical metrics for model evaluation

The mean bias (*MB*), normalized mean bias (*NMB*), normalized mean error (*NME*), and root mean square error (*RMSE*) calculated based on simulation results and observation data, were used to evaluate the CMAQ model performance. The calculations of the *MB*, *NMB*, *NME* and *RMSE* are defined by equations (3) - (6), respectively. The *M* represents the model results, *O* represents the observations, and *N* represents the number of data points.

$$MB = \frac{1}{N}\sum_{i=1}^{N}\left(M_i - O_i\right) \qquad (3)$$

$$NMB = \frac{\sum_{i=1}^{N}\left(M_i - O_i\right)}{\sum_{i=1}^{N} O_i} \times 100\% \qquad (4)$$

$$NME = \frac{\sum_{i=1}^{N}\left|M_i - O_i\right|}{\sum_{i=1}^{N} O_i} \times 100\% \qquad (5)$$

$$RMSE = \left[\frac{1}{N}\sum_{i=1}^{N}\left(M_i - O_i\right)^2\right]^{\frac{1}{2}} \qquad (6)$$

3 Results and discussion

3.1 Evaluation of model performance

The capability of the WRF model to reproduce meteorological conditions has already been evaluated by comparison with observations at 824 national meteorological sites in China

and it is described in much greater details in Wu et al. (2020). They found that the 2-m temperature and downward shortwave radiation were generally well reproduced by the WRF model, although both were slightly underestimated likely owing to overestimation of the cloud coverage.

The simulated $PM_{2.5}$ concentrations in all scenarios by CMAQ model were evaluated against observations in 74 cities (536 sites in total) from the national monitoring network operated by the China National Environmental Monitoring Center (CNEMC). The hourly $PM_{2.5}$ mass concentrations are measured using the micro-oscillating balance method and/or the β absorption method (MEE, 2012). Daily average $PM_{2.5}$ values are used to compare the measurements against simulations. The MB, NMB, NME and RMSE are calculated to evaluate the model performance on $PM_{2.5}$ concentration at the monitoring sites, as shown in Table 3.

The model results from the base scenario reasonably agree with observed $PM_{2.5}$ concentrations, with MB of 1.7 μg m^{-3} and -5.5 μg m^{-3}, NMB of 10.3% and -12.4%, NME of 36.8% and 42.0%, and RMSE of 22.3 μg m^{-3} and 30.1 μg m^{-3} for summer and winter, respectively. The CMAQ model performance in this study compares well with other studies (Hu et al., 2016). The model performance in summer is somewhat better than for the winter, with the model predicted wintertime $PM_{2.5}$ systematically lower than the observations for winter. This seasonal difference may be attributed to allocation bias for emission inventories and challenges in simulating relevant changes in meteorological conditions (B. Zheng et al., 2015). Overall, the base case CMAQ simulation reproduced the seasonally averaged $PM_{2.5}$ concentration successfully and the spatial pattern of simulated $PM_{2.5}$ concentration agrees well with observations over China. However, it should be noted that NH_3 is not the criteria pollutant monitored by the CNEMC network and the NH_3 observations of Ammonia Monitoring Network-China (AMoN-China) were not publicly available, thus there was not monitoring data of NH_3 can be used to compare against modeled NH_3 levels by CMAQ simulations. Nonetheless, the MEIC emission inventory for the year of 2016 used in this study was the closest year with updated information on local emission activities and emission factors across China. Extensive studies have been conducted to evaluate the NH_3 emissions in MEIC inventory and those results show excellent agreement with satellite-derived NH_3 column and ambient NH_3 measurements (Kong et al., 2019; M. Li et al., 2017; L. Zhang et al., 2018; Q. Zhang et al., 2019). Additional

investigation focused on evaluating the modeled NH_3 mixing ratio against observations should be considered in future work.

When the process of NH_3 uptake to SOA was included, the simulated $PM_{2.5}$ concentrations decreased in both seasons, with the magnitude of the decrease increasing with the assumed uptake coefficient. For winter, this exacerbated the underestimation of $PM_{2.5}$, with the NMB changing from -12.4% (base case) to -18.6% ($\gamma = 10^{-3}$). For summer, the simulated $PM_{2.5}$ in base case exceeded the observed value. Consequently, the small overestimation in summertime $PM_{2.5}$ for the base case decreased with NH_3-SOA uptake, with best agreement for the $\gamma = 10^{-4}$ scenario; when $\gamma = 10^{-3}$, the model underestimates the summertime $PM_{2.5}$. In the sections that follow, the specific factors that control these changes in the total $PM_{2.5}$ concentrations are examined.

Table 3. Comparison between simulation results for $PM_{2.5}$ and observations from the CNEMC monitoring network for seasonal averages. (Obs. stands for observation. Sim. stands for simulation).

Scenario	Period	Obs.mean $\mu g\ m^{-3}$	Sim.mean $\mu g\ m^{-3}$	MB $\mu g\ m^{-3}$	NMB %	NME %	RMSE $\mu g\ m^{-3}$
Base	Summer	28.5	30.2	1.7	10.3	36.8	22.3
$\gamma = 10^{-5}$	Summer	28.5	29.6	1.1	8.7	44.9	18.2
$\gamma = 10^{-4}$	Summer	28.5	28.3	-0.2	-2.8	33.0	15.9
$\gamma = 10^{-3}$	Summer	28.5	26.4	-2.1	-6.4	52.4	36.8
Base	Winter	74.0	68.5	-5.5	-12.4	42.0	30.1
$\gamma = 10^{-5}$	Winter	74.0	67.4	-6.6	-14.9	46.8	33.2
$\gamma = 10^{-4}$	Winter	74.0	66.9	-7.1	-17.1	49.1	36.0
$\gamma = 10^{-3}$	Winter	74.0	63.7	-10.3	-18.6	52.3	42.1

3.2 Base case spatial distribution of simulated ammonia mixing ratio

There is substantial spatial variability in the simulated NH_3 mixing ratio, and a large difference between summer and winter (Figure 2). In particular, the NH_3 mixing ratio is more than doubled in summer than in winter due to the elevated anthropogenic emissions and higher temperature, which promotes the NH_3 emission from vegetation and fertilized soils (Meng et al., 2018). In summer, high NH_3 mixing ratio are observed over southwestern China (the Sichuan Basin) and central China (Hebei, Shandong and Henan provinces), reflecting intensive agricultural activities over these areas. Besides, there are also some NH_3 hotspots in the North China Plain (including Beijing, Tianjin, Hebei, Shandong, eastern Henan and northern Anhui

regions). According to national estimation from the Ministry of Ecology and Environment of China (MEE), the fertilizer used in these regions exceeds 30% of the total national consumption (Gu et al., 2015). Additionally, intensive livestock framing also contributes to the high NH_3 mixing ratio in the North China Plain (Bai et al., 2018; Gao et al., 2013). In winter, some highly localized ammonia hotspots pop up in eastern China (See Figure 2b). In addition to the regions in southwestern China and central China, it should be noted that high NH_3 mixing ratio are also observed over northeastern China and, to a lesser extent, the province of Xinjiang in Northwest China in both seasons, likely from animal grazing related emissions. The seasonal variation and location of NH_3 hotspots are consistent with the findings reported by L. Zhang et al. (2018) and Kong et al. (2019), which backs up our emission inventory and simulation results.

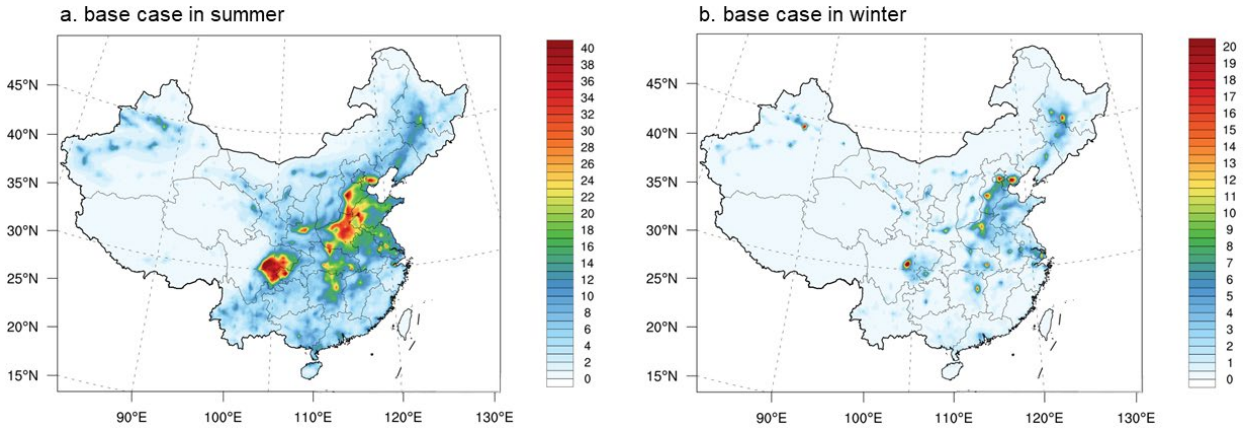

Figure 2. Spatial distribution of simulated surface NH_3 mixing ratio (unit: ppb) in the base case for (a) summer and (b) winter.

3.3 Impact of ammonia uptake on gas-phase NH_3 and HNO_3

The impact on NH_3 mixing ratio and HNO_3 concentration due to NH_3-SOA uptake is presented in Figure 3, with the difference between the base case and the $\gamma = 10^{-3}$, 10^{-4} and 10^{-5} cases. The NH_3 mixing ratio are found decreased when including the NH_3-SOA uptake mechanism. The magnitude of reduction increased as the uptake coefficient increase. Specifically, in the summer, the spatially averaged NH_3 mixing ratio for the base case is 1.49 ppb. For the largest uptake coefficient considered, $\gamma = 10^{-3}$, the summertime spatially averaged NH_3 mixing ratio decreased to 1.08 ppb (-27.5 %). For the $\gamma = 10^{-4}$ and $\gamma = 10^{-5}$ cases, the NH_3 mixing ratio decreased to 1.36 ppb (-8.8%) and 1.46 ppb (-2.0%), respectively. In the wintertime,

the spatiotemporally averaged NH_3 mixing ratio for the base case is 0.21 ppb, it decreases to 0.20 ppb (−4.8 %) for $\gamma = 10^{-5}$, 0.19 ppb (−9.5 %) for $\gamma = 10^{-4}$, and 0.17 ppb (−19.0 %) for $\gamma = 10^{-3}$. After applying the NH_3-SOA uptake mechanism, NH_3 mixing ratio in the North China Plain (including Beijing, Tianjin, Hebei, Shandong, eastern Henan and northern Anhui regions) decreased significantly both in summer and winter. Spatially, the maximum decreases of NH_3 mixing ratio occur in regions where the ammonia mixing ratio is highest (see Figure 2). The largest decrease occurred in the North China Plain. The decrease of NH_3 mixing ratio resulting from its uptake to SOA is also significant in the Sichuan Basin, which has the second highest NH_3 emissions after the North China Plain, reflecting the dense livestock farming in this area. Some regions in Hunan, Hubei and Henan provinces also shows decreases in NH_3 mixing ratio.

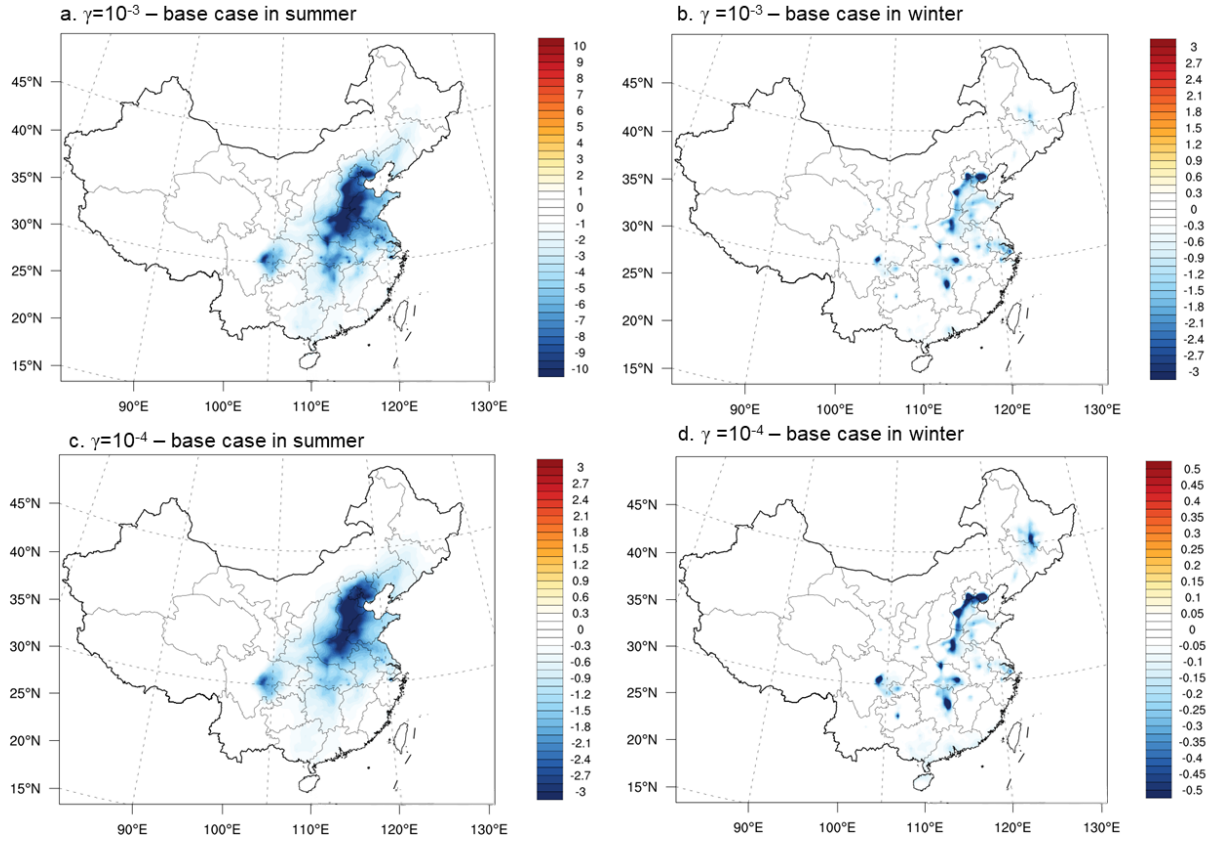

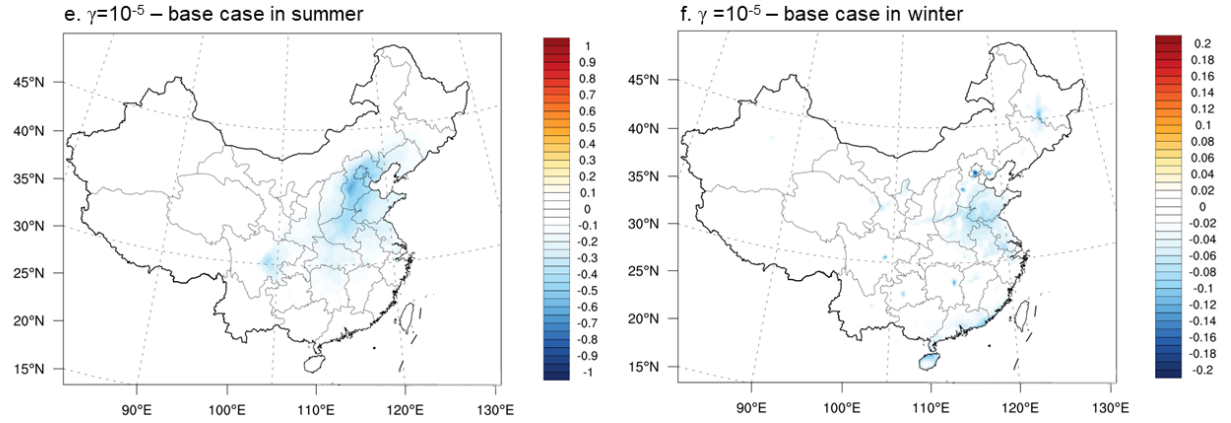

Figure 3. Spatial distribution of the difference in surface NH_3 mixing ratio (unit: ppb) between the $\gamma = 10^{-3}$ case, $\gamma = 10^{-4}$ case, $\gamma = 10^{-5}$ case and the base case for summer and winter. Negative values represent decreases in mixing ratio compared with the base case.

The gas-particle partitioning of HNO_3 directly depends on the relative abundance of NH_3. For constant total nitrate ($HNO_{3(g)} + NO_3^-{}_{(p)}$), it is expected that the gas-phase HNO_3 concentration will increase in response to decreased NH_3 mixing ratio. The base case simulation results show strong seasonal variation in HNO_3 concentration, reflecting differences in NO_x emissions, production and loss pathways, and gas-particle partitioning (Figure 4). In summer, the HNO_3 concentrations are highest in the North China Plain and northern region of Henan Province. In winter, the highest HNO_3 concentrations mainly occur in southern Sichuan Basin and southern China.

Figure 5 shows the difference of HNO_3 levels between the base case and three NH_3 uptake scenarios for summer and winter. In summer, the average percent change in the HNO_3 concentration is 5.7% for $\gamma = 10^{-3}$, 1.5% for $\gamma = 10^{-4}$, and 0.6% for $\gamma = 10^{-5}$. In winter, the average percent increase in the HNO_3 concentration is 9.3% for $\gamma = 10^{-3}$, 1.9% for $\gamma = 10^{-4}$, 1.2% for $\gamma = 10^{-5}$. For all the NH_3 uptake cases, the HNO_3 concentrations in the North China Plain increased, corresponds to the significant NH_3 reduction in this region (Figure 3). In summer, the HNO_3 concentrations peaks over the North China Plain thus the change of magnitude also reaches highest in the North China Plain due to the NH_3 reduction. However, the spatial pattern of HNO_3 concentrations over the North China Plain is quite different between winter and summer, where a substantial increase in HNO_3 emerged in the North China Plain even though the absolute HNO_3 concentrations is low in this region. And the similar pattern is also found over Henan and

Shandong Province. This phenomenon can be attributed to high NO_x emissions across these regions with low NH_3 mixing ratio in winter which promotes gas-phase HNO_3 accumulation (Fu et al., 2020). Additionally, this condition also illustrated that the HNO_3 concentrations over these regions are more sensitive to changes in NH_3 compared with other regions.

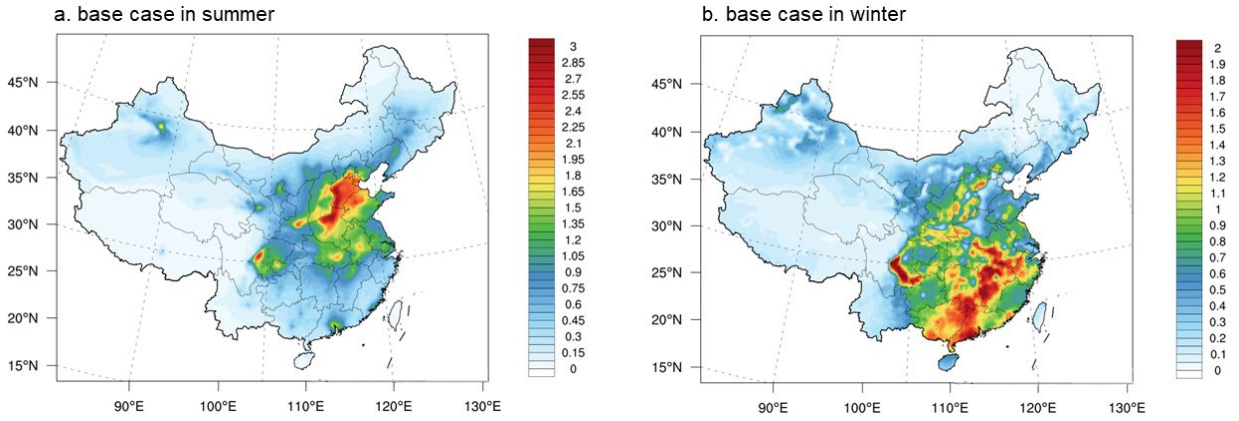

Figure 4. Spatial distribution of simulated surface HNO_3 concentrations (unit: μg m^{-3}) in the base case for (a) summer and (b) winter.

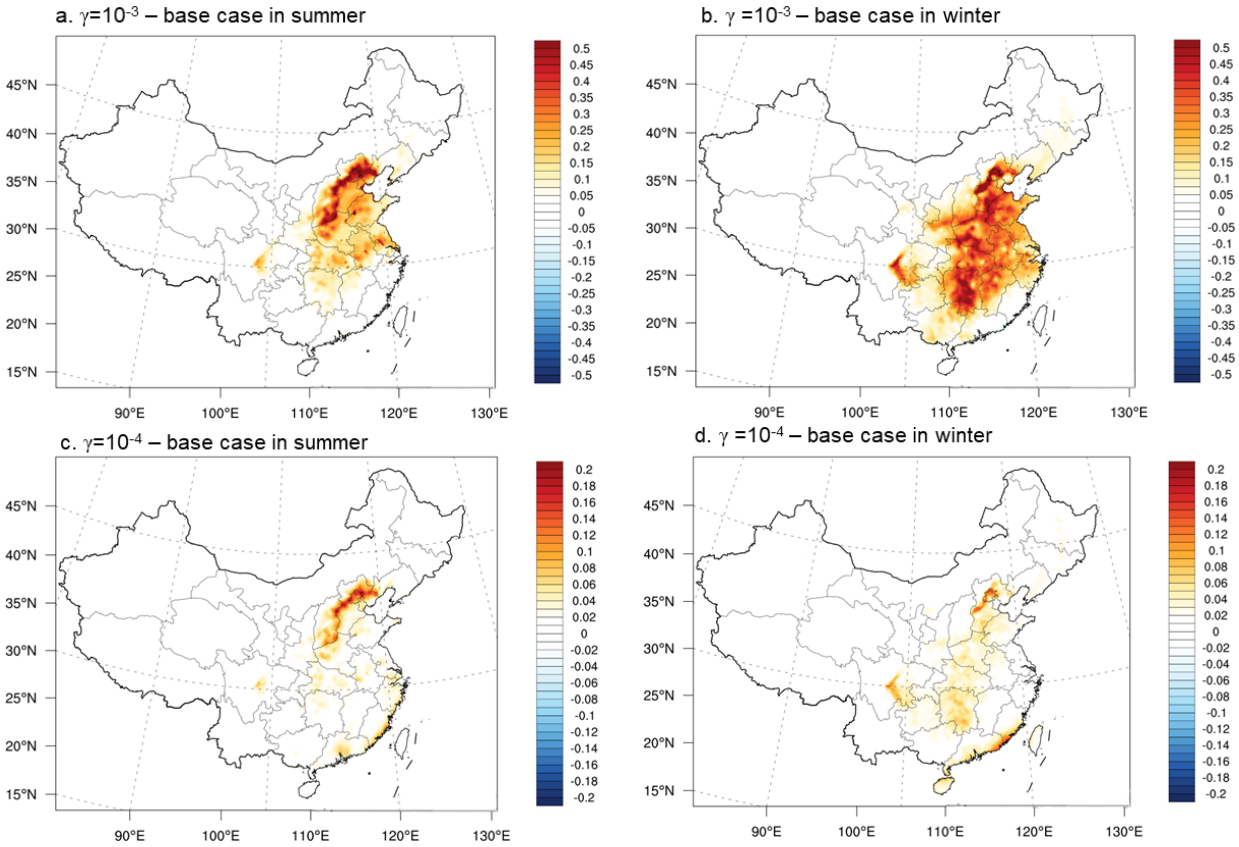

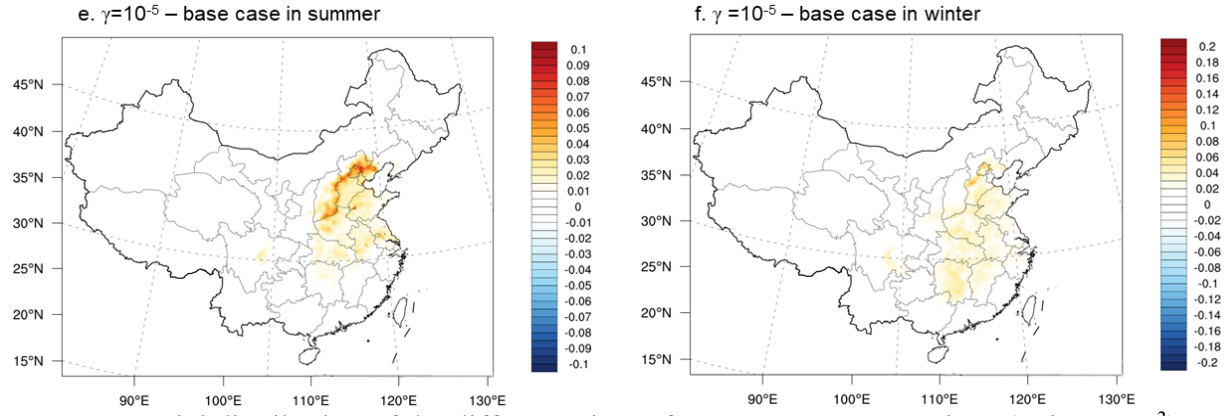

Figure 5. Spatial distribution of the difference in surface HNO_3 concentrations (unit: μg m^{-3}) between the $\gamma = 10^{-3}$ case, $\gamma = 10^{-4}$ case, $\gamma = 10^{-5}$ case and the base case for summer and winter. Negative values represent decreases in concentration compared with the base case.

3.4 Impact of ammonia uptake on inorganic PM

As noted above, changes in gas-phase NH_3 mixing ratio influence the gas-particle partitioning of atmospheric compositions, such as HNO_3 and H_2SO_4. The spatial distribution of simulated surface NH_4^+ concentrations in the base case are shown in Figure 6. In summer, high NH_4^+ concentrations are found in the Sichuan Basin, Shandong Province and North China Plain. There are some hotspots presented in Henan, Hubei and Hunan Provinces. It is noteworthy that the summertime distribution of NH_4^+ is similar with the distribution of combination of the NH_3 and HNO_3 maps, which indicate sufficient NH_3 neutralizers (e.g., HNO_3 and H_2SO_4) and abundant NH_3 emissions from intensive agricultural activities (as shown in Figure 2). In winter, the Sichuan Basin, eastern and central China exhibits high NH_4^+ concentrations, largely due to the enhanced anthropogenic emissions. Compared with the NH_3 distribution in winter, the spatial distribution of NH_4^+ concentrations in winter is spreading out more than the NH_3 owing to the longer lifetime of NH_4^+ compared to NH_3.

Figure 7 compares the difference in NH_4^+ concentrations between the $\gamma = 10^{-3}$ case, $\gamma = 10^{-4}$ case, $\gamma = 10^{-5}$ case and the base case for summer and winter. The reduction in gas-phase NH_3 from uptake to SOA, which converts NH_3 to NOCs, results in a decrease in particle phase NH_4^+. The NH_3 uptake caused NH_4^+ concentrations to decrease in most areas of China. In summer, the average percent decrease in NH_4^+ is 4.0% for $\gamma = 10^{-5}$, 8.0% for $\gamma = 10^{-4}$, and 20.0% for $\gamma = 10^{-3}$ while the average percent decrease is 1.7 % for $\gamma = 10^{-5}$, 3.4 % for $\gamma = 10^{-4}$, and 13.8% for $\gamma = 10^{-3}$ in winter, respectively.

Figure 8 presents the simulated SO_4^{2-} concentrations in the base case. In summer, high SO_4^{2-} concentration peaks in Sichuan Basin and there are some hotspots distributed in eastern China and central China. In winter, the $(NH_4)_2SO_4$ concentration was higher over the southwestern and central China compared with the summer, indicating that there is sufficient NH_3 to neutralize most H_2SO_4 in these regions because NH_3 is first neutralized by the H_2SO_4 in the presence of HNO_3 and H_2SO_4. It should be noted that the impacts of NH_3 uptake on SO_4^{2-} concentrations in all scenarios are very small (Figure not shown) because of the rich NH_3 environment which makes SO_4^{2-} insensitive to moderate changes in NH_3.

In contrast to sulfate, the NH_3 decrease from uptake to SOA can have a notable impact on the gas-particle partitioning of the weaker acid HNO_3 and the particulate nitrate concentrations. Figure 9 presents the spatial distribution of simulated surface NO_3^- concentrations in the base case for summer and winter. In summer, the areas with high NO_3^- concentrations of ~5 $\mu g\ m^{-3}$ are limited to the North China Plain and the Sichuan Basin while all other regions have concentrations less than 3 $\mu g\ m^{-3}$. In winter, the NO_3^- concentrations are much higher than summer, reaching approximately 20 $\mu g\ m^{-3}$ in the North China Plain, the Yangtze River Delta, and central China. Compared to the spatial distribution of SO_4^{2-}, which generally occurs as localized hotspots located in the Sichuan Basin and northeastern China, NO_3^- pollution is more widely distributed, especially in the North China Plain, Yangtze River Delta and the Sichuan Basin. This phenomenon likely reflects different sources, lifetimes, and conversion processes for SO_2 and NO_2 (see Figure S2). Figure 10 shows the spatial distributions of the difference between the NH_3 uptake scenarios and the base case for NO_3^- for winter and summer. Compared with the changes in NH_4^+, greater percent changes are observed for NO_3^-, especially in winter. In summer, the average percent decrease in NO_3^- is 8.1% for $\gamma = 10^{-5}$, 13.5% for $\gamma = 10^{-4}$, and 29.7% for $\gamma = 10^{-3}$ while in winter the average decrease is 3.0 % for $\gamma = 10^{-5}$, 4.0 % for $\gamma = 10^{-4}$, and 15.0% for $\gamma = 10^{-3}$. While the absolute magnitudes of the changes depend on the assumed γ, the spatial patterns of the changes are similar between the cases. In general, the reduction of NO_3^- mainly concentrated in regions with high NO_3^- concentrations, such as North China Plain, Yangtze River Delta and central China. However, neither NH_4^+ concentrations nor NO_3^- concentrations change much in the Sichuan Basin where NH_3 mixing ratio are very high. This may be associated with the source emission to form NO_3^- is very low compared to NH_3. Besides, it should be noted that the decrease in NH_4^+ is much larger around Hubei and Henan provinces than it is in the Sichuan

Basin, which illustrated the regional differences in sensitivity response of NH_4^+ and NO_3^- to the reduction in NH_3.

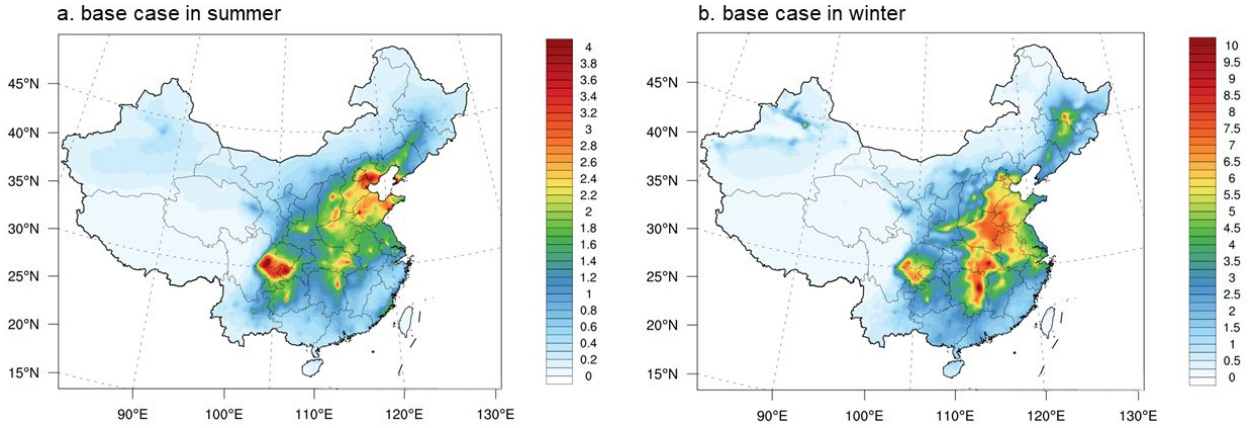

Figure 6. Spatial distribution of simulated surface NH_4^+ concentrations (unit: μg m^{-3}) in the base case for (a) summer and (b) winter.

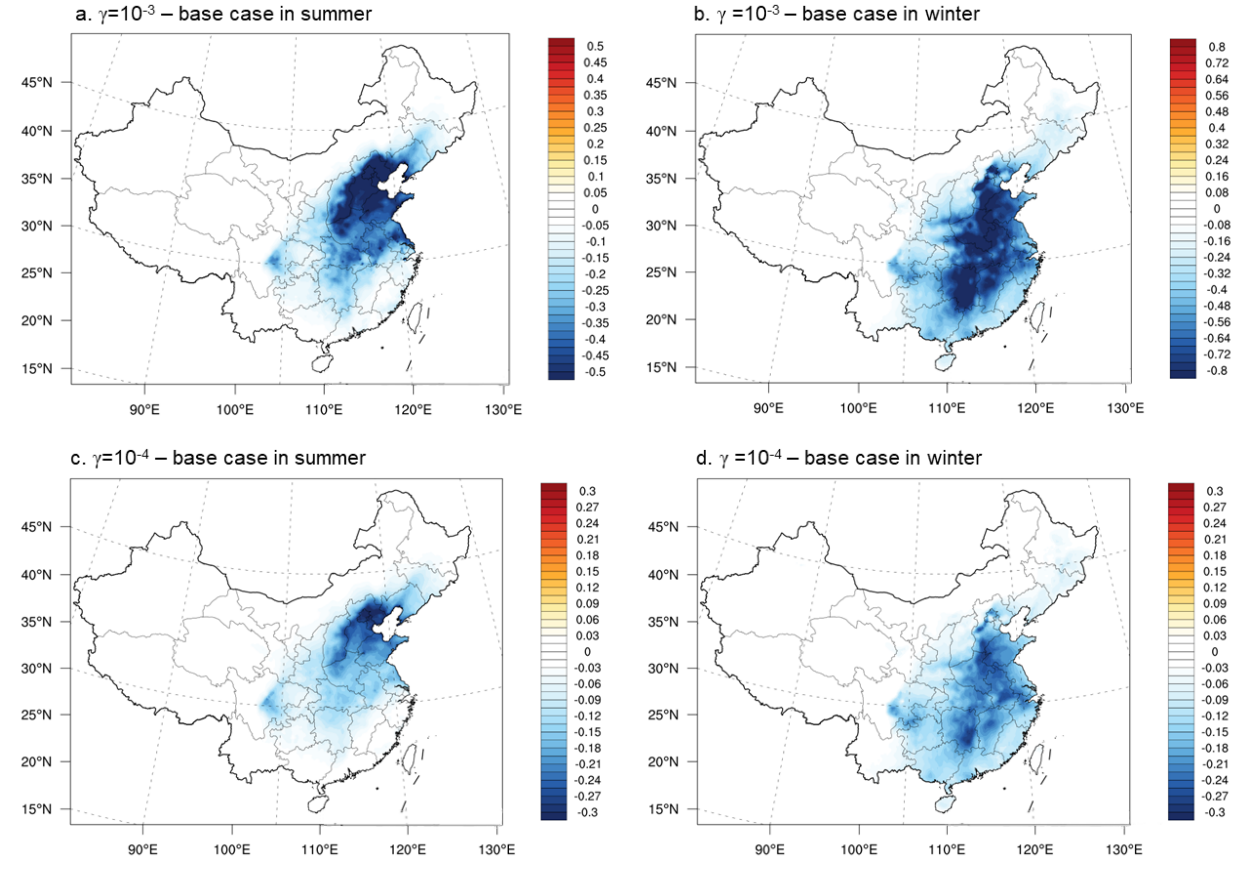

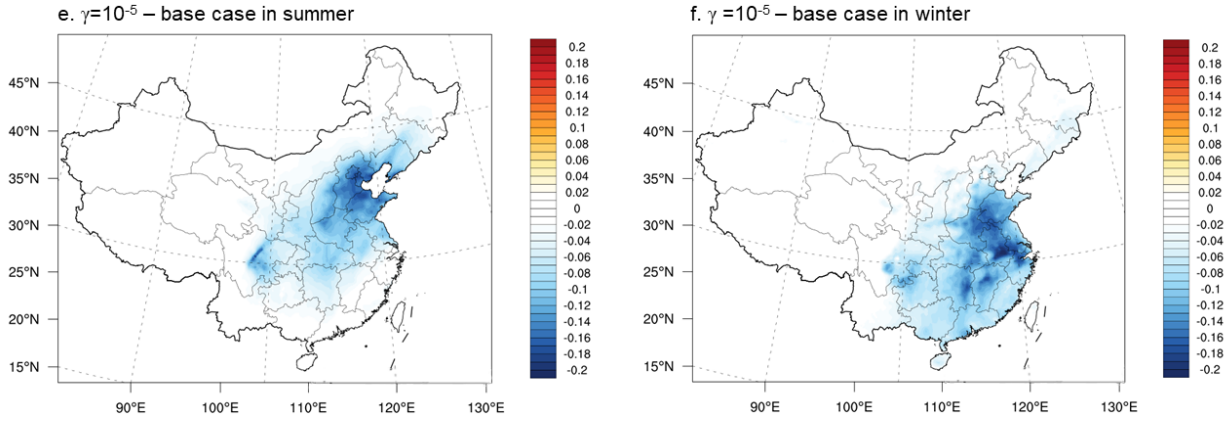

Figure 7. Spatial distribution of the difference in surface NH_4^+ concentrations (unit: μg m^{-3}) between the $\gamma = 10^{-3}$ case, $\gamma = 10^{-4}$ case, $\gamma = 10^{-5}$ case and the base case for summer and winter. Negative values represent decreases in concentration compared with the base case.

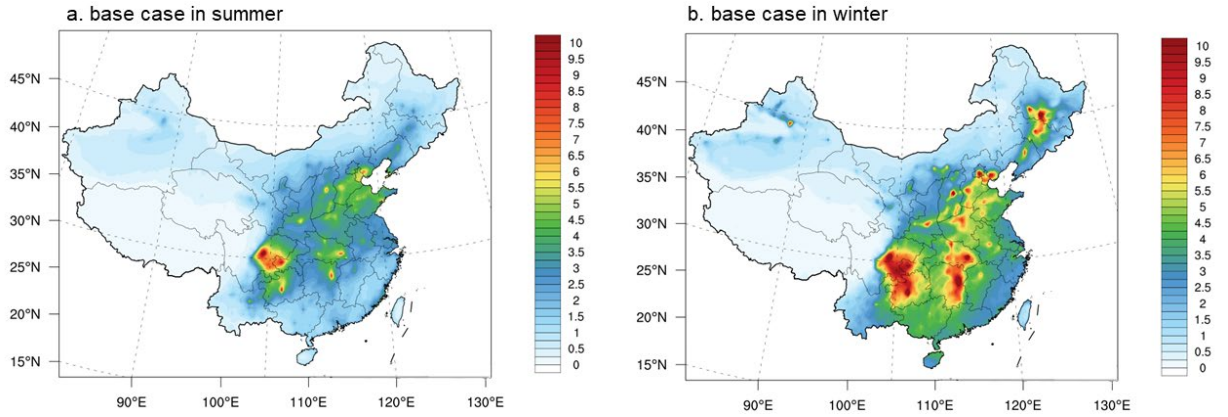

Figure 8. Spatial distribution of simulated surface SO_4^{2-} concentrations (unit: μg m^{-3}) in the base case for (a) summer and (b) winter.

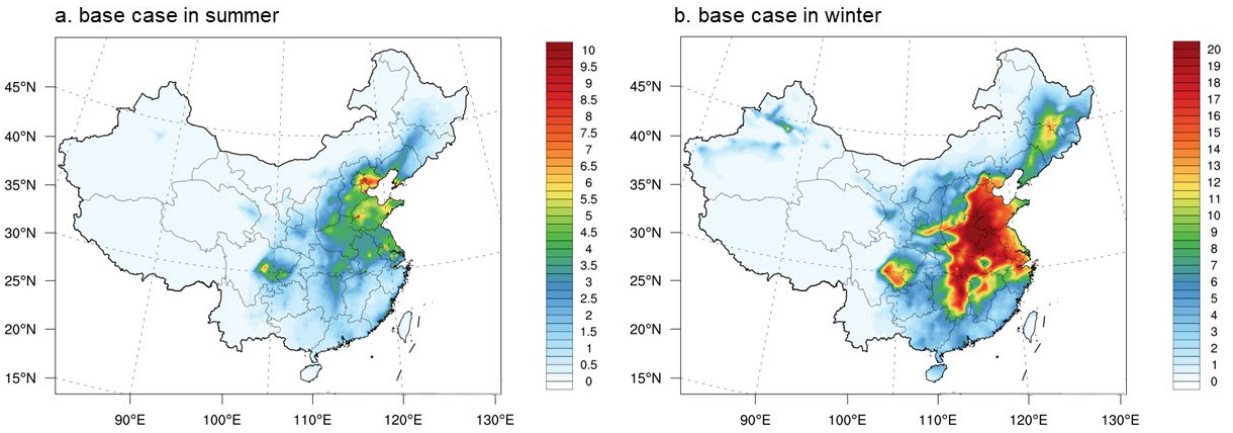

Figure 9. Spatial distribution of simulated surface NO_3^- concentrations (unit: μg m^{-3}) in the base case for (a) summer and (b) winter.

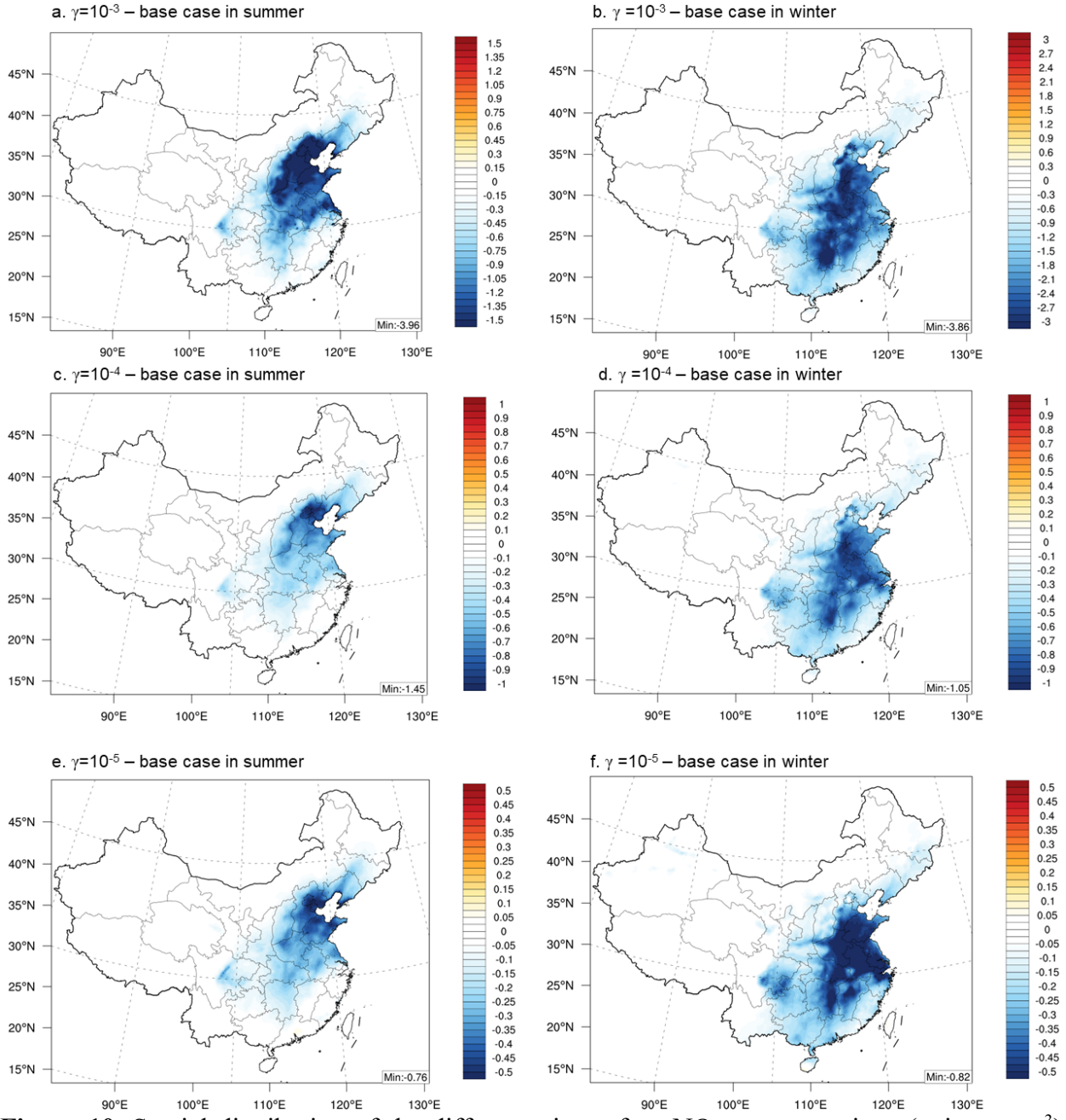

Figure 10. Spatial distribution of the difference in surface NO_3^- concentrations (unit: μg m^{-3}) between the $\gamma = 10^{-3}$ case, $\gamma = 10^{-4}$ case, $\gamma = 10^{-5}$ case and the base case for summer and winter. Negative values represent decreases in concentration compared with the base case.

3.5 Impact of ammonia uptake on secondary organic aerosol

Figure 11 shows the time-averaged spatial distribution of SOA in the base cases. In summer, the simulated SOA concentrations are largest in the Sichuan Basin, North China Plain, and central China, with SOA concentrations reaching more than 12 μg m^{-3}. The high SOA concentrations in these regions can be partly attributed to strong biogenic VOC emissions, which plays an essential role in SOA formation in summer (Qin et al., 2018; Wu et al., 2020). In addition, the high temperature and strong solar radiation in summer also favors faster photochemical production of SOA over China. In winter, the highest SOA concentrations reach over 20 μg m^{-3} in the Sichuan Basin, northeastern and central China. Other populated areas in the North China Plain, Pearl River Delta, and Hunan and Hubei provinces have SOA concentrations in the range of 8-10 μg m^{-3} in winter. For the North China Plain and northeastern China, the wintertime SOA is largely attributed to the enhanced residential emissions of VOCs especially from coal combustion related to cooking and collective heating (Wang et al., 2018). For the Sichuan Basin and other regions located in southern China, high wintertime SOA concentrations are mainly caused by the joint effects of industrial emissions and unfavorable meteorological conditions which are characterized by high relative humidity, low atmospheric boundary layer height, and weak winds (Yang et al., 2020).

Even though the direct effect of the NH_3 uptake parameterization applied in this study on SOA concentration should be small, as the NH_3 uptaken is offset by the water loss. However, the changes in chemical composition could alter the particle acidity, which can indirectly influence SOA concentration by changing the rate of acid-catalyzed heterogeneous reactions associated with SOA formation from isoprene oxidation products (Pye et al., 2013). Figure 12 illustrates the difference in SOA concentrations between the $\gamma = 10^{-3}$ case, $\gamma = 10^{-4}$ case, $\gamma = 10^{-5}$ case and the base case for summer and winter. In all scenarios, the implementation of NH_3 uptake mechanism has little influence on the SOA concentration. Interestingly, unlike the SIA components that only decrease, the SOA concentrations can either increase or decrease with consideration of NH_3-SOA uptake. In summer, NH_3 uptake results to slight decreases in SOA concentrations over the Sichuan Basin and central China for all γ, but the SOA concentrations increase by 10% for the southeast region, including Zhejiang, Fujian and Jiangxi provinces, when $\gamma = 10^{-3}$. In winter, there are slight increases in SOA concentrations over the Sichuan Basin, the North China Plain and northeastern China while the SOA concentrations decrease slightly in southern China.

These changes are related to the variation of isoprene-derived SOA formation caused by the change of particle pH, shown in Figure 13 and Figure S3. In summer, the particle pH increased by about 1 pH unit for the $\gamma = 10^{-3}$ scenario in Yangtze River Delta, Pearl River Delta, Fujian, Xinjiang, Tibet and some other western provinces, while the particle pH decreased in the North China Plain and northeastern China. This may be attributed to the differences of the dominant chemical components in $PM_{2.5}$ over these regions. Even though large changes in pH occur over western China which shows very low SOA concentrations (Xinjiang, Tibet and some other western provinces), the NH_3 uptake process is expected to have little impact on the absolute SOA due to the low SOA concentrations in these regions. In winter, most regions show decreases in particle pH for the $\gamma = 10^{-3}$ scenario especially in the North China Plain, northeastern China, the Sichuan Basin and other southern provinces. Therefore, the small increase of SOA concentration in these regions is attributed to the reduction of pH, which enhanced acid-catalyzed heterogeneous reactions for isoprene. It should be noted that the changes observed in winter are as large as in summer even though the isoprene emissions are very low in winter compared to summer. As isoprene is the only SOA forming species that depends on acidity in CMAQ simulation, this phenomenon implies potentially notable changes in the isoprene-derived SOA contribution in winter due to the NH_3 uptake effects. While notable effects of pH changes on SOA were found when $\gamma = 10^{-3}$, the changes in pH for the $\gamma = 10^{-4}$ and $\gamma = 10^{-5}$ scenarios were overall relatively small (<0.4 pH units), whereas associated changes for $\gamma = 10^{-4}$ and $\gamma = 10^{-5}$ scenarios in the SOA concentrations are as large as $\gamma = 10^{-3}$. Overall, the impacts of NH_3 uptake mechanism on SOA are not as obvious as for inorganic aerosol. It is noteworthy that these results further support the finding of Guo et al. (2018), who pointed out that the reduction of NH_3 mixing ratio will not lead to a large decrease in particle pH because of the high sulfate production over China..

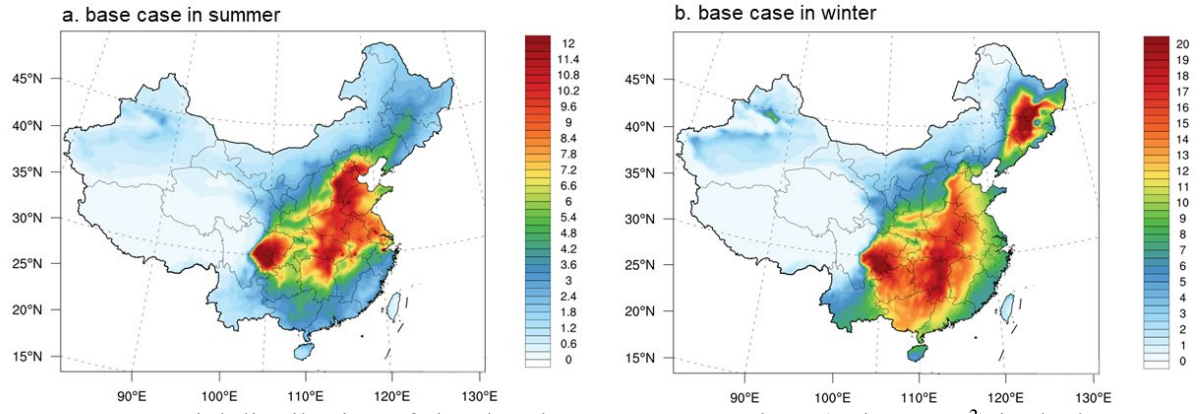

458
459 **Figure 11.** Spatial distribution of simulated SOA concentrations (unit: μg m^{-3}) in the base case for
460 (a) summer and (b) winter.
461

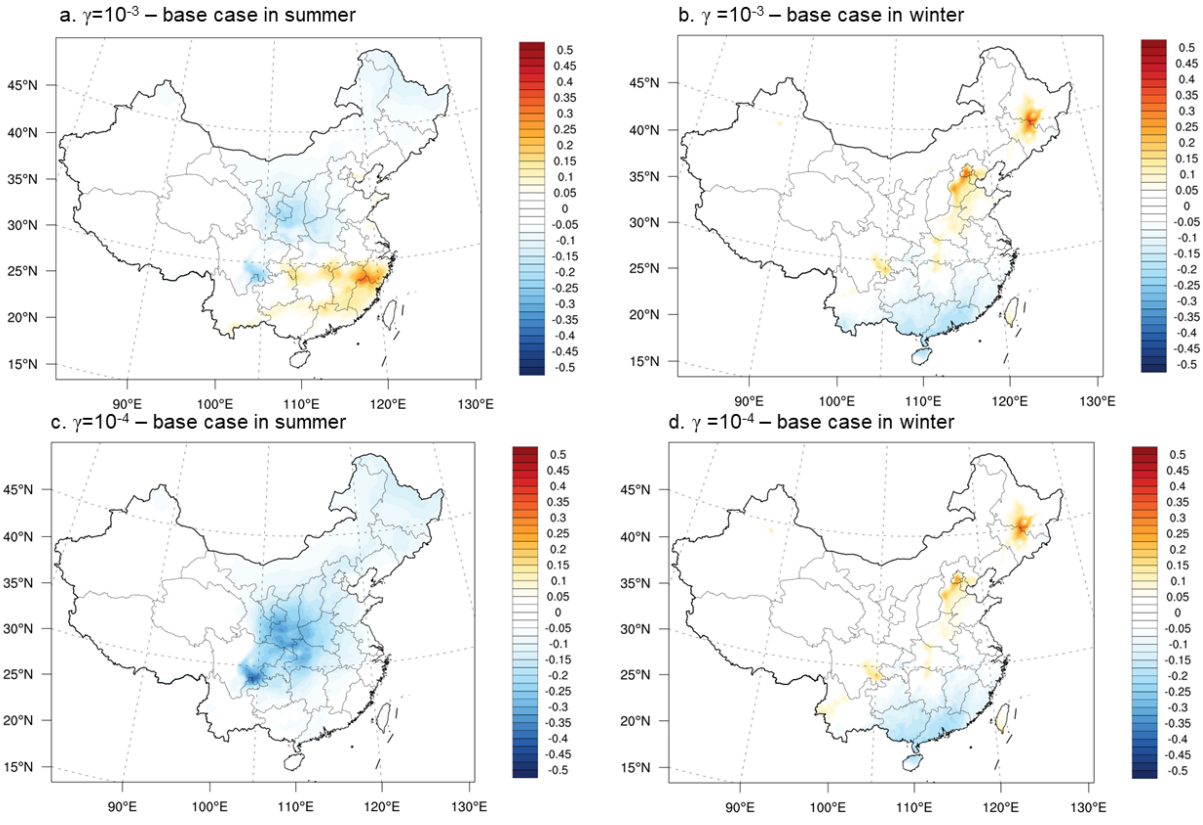

462

463
464

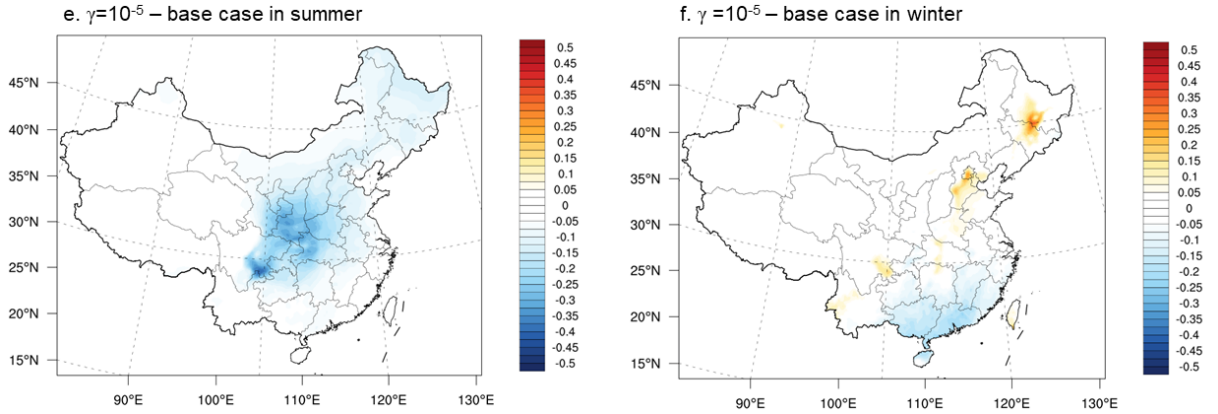

Figure 12. Spatial distribution of the difference in surface SOA concentrations (unit: μg m^{-3}) between the $\gamma = 10^{-3}$ case, $\gamma = 10^{-4}$ case, $\gamma = 10^{-5}$ case and the base case for summer and winter. Negative values represent decreases in concentration compared with the base case.

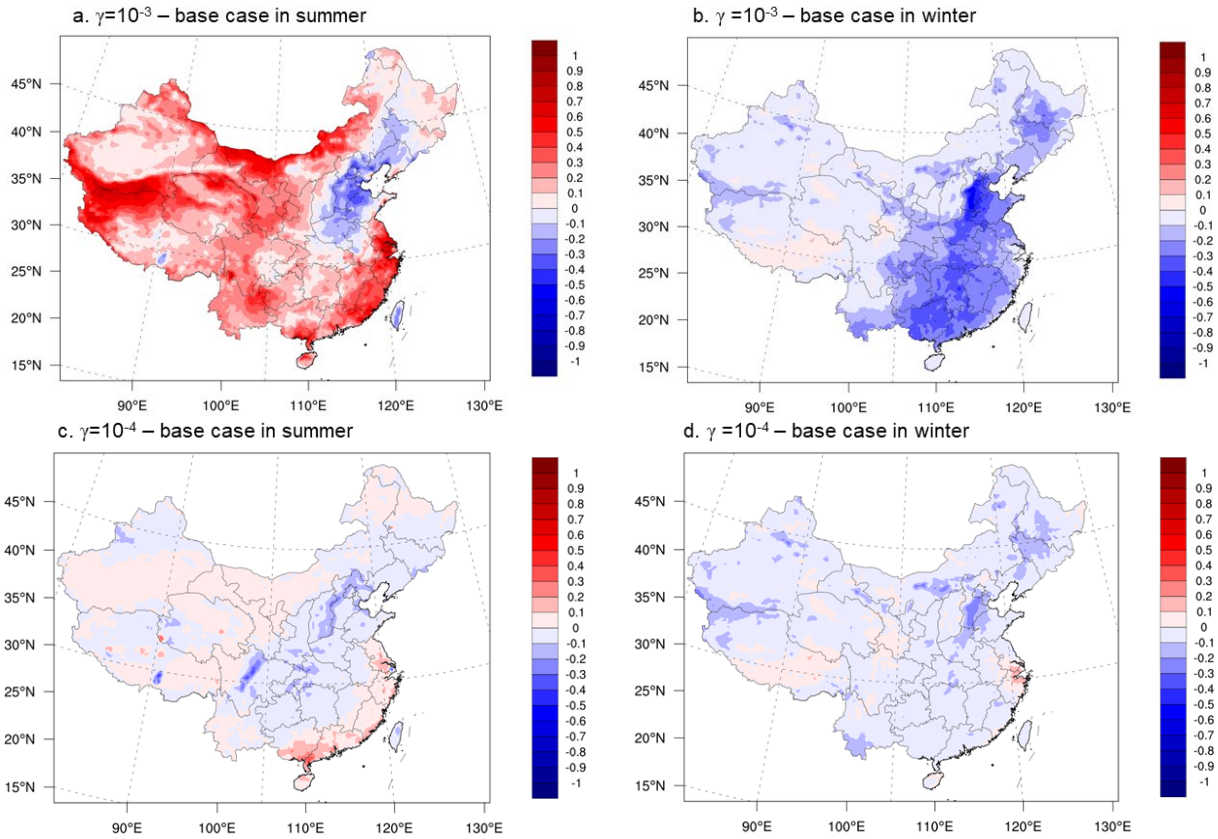

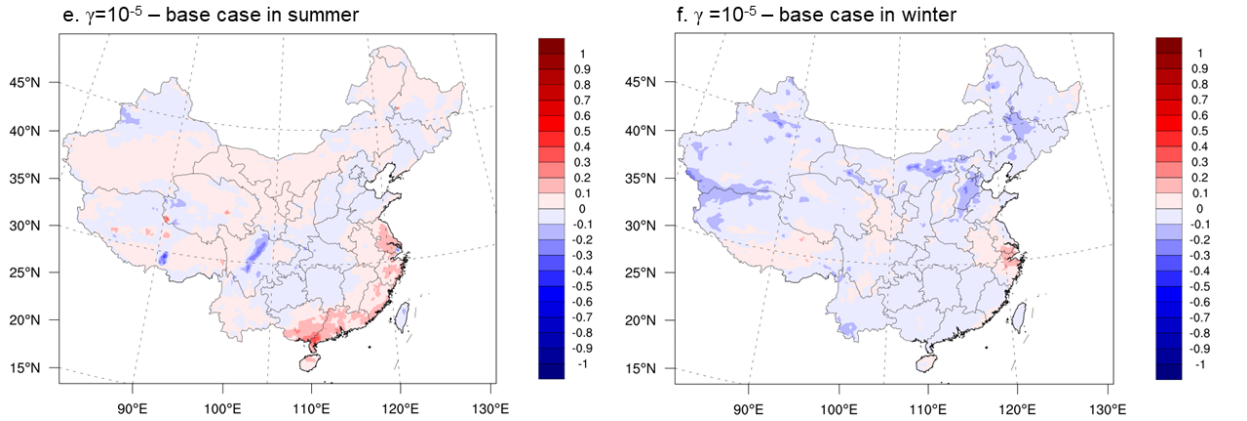

Figure 13. Spatial distribution of the difference in particle pH between the $\gamma = 10^{-3}$ case, $\gamma = 10^{-4}$ case, $\gamma = 10^{-5}$ case and the base case for summer and winter. Negative values represent decreases in concentration compared with the base case.

3.6 Impact of ammonia uptake on total PM

The spatial distribution of time-averaged $PM_{2.5}$ concentration in summer and winter is presented in Figure 14. The simulated $PM_{2.5}$ concentration in winter is much higher than in summer due to the enhanced anthropogenic emissions and meteorological conditions. In winter, the primary emissions of elemental carbon, organic carbon, VOCs and NO_2 especially from transportation and residential sources are much higher than summer. Besides, the low planetary boundary layer height and frequent temperature inversions occurred in winter which often associated with winter stagnant conditions, is unfavorable for the ventilation of $PM_{2.5}$. Furthermore, stronger rainfall in the summer induced by the monsoon would greatly reduce the aerosol lifetimes compared to winter. In summer, high $PM_{2.5}$ concentrations of ~30 μg m^{-3} mainly concentrated over eastern China, the North China Plain and the Sichuan Basin while all other regions have concentrations of < 20 μg m^{-3}. These $PM_{2.5}$ hotspots are highly related to the large fraction of ammonium sulfate and ammonium nitrate in $PM_{2.5}$ in these regions (as discussed in Section 4.3). In addition, biogenic SOA also contributes significantly to the high $PM_{2.5}$ concentrations over central China and the Sichuan Basin (Wu et al., 2020). In winter, high $PM_{2.5}$ concentrations over 70 μg m^{-3} are simulated in the North China Plain, the Sichuan Basin, central China and northeastern China. The high $PM_{2.5}$ in the North China Plain can be attributed to unfavorable meteorological conditions in wintertime including stable synoptic weather patterns and persistent high relative humidity which could promote the secondary transformation

of gaseous pollutants (Cheng et al., 2019; H. Zhang et al., 2019; Y. Zhang et al., 2016). In addition, emissions of primary pollutants is increased especially from transportation and coal-burning sources (G. J. Zheng et al., 2015). The hotspots simulated over the Sichuan Basin are caused by frequent stagnant weather conditions and blockage of dispersion due to basin topography (Liao et al., 2018; Yang et al., 2020). It should be noted that the $PM_{2.5}$ concentrations in northeastern China are very high with average concentrations reaching over 70 μg m^{-3} in winter. In addition to the impacts of meteorological conditions, such as stable atmospheric boundary layer and high relative humidity which favors the hygroscopic growth of particles (Z. Chen et al., 2018; Sun et al., 2016), these high concentrations also result from combined emissions of strong open biomass burning and residential heating (X. Li et al., 2017).

Figure 15 shows the differences in $PM_{2.5}$ concentrations between the $\gamma = 10^{-3}$ case, $\gamma = 10^{-4}$ case, $\gamma = 10^{-5}$ case and the base case for summer and winter. In summer, the average decrease in $PM_{2.5}$ concentrations is 6.6% for $\gamma = 10^{-5}$, 8.3% for $\gamma = 10^{-4}$, and 8.9% for $\gamma = 10^{-3}$ while the average decrease is 5.3 % for $\gamma = 10^{-5}$, 8.1 % for $\gamma = 10^{-4}$, and 8.7% for $\gamma = 10^{-3}$ in winter respectively. As shown in Figure 15, the $PM_{2.5}$ concentrations decreased across the whole domain. In summer, the Sichuan Basin and the North China Plain show the largest decrease magnitude in $PM_{2.5}$ concentrations. In winter, the largest reductions occurred over eastern China and the Sichuan Basin. These reductions are mainly attributed to the decrease in NH_4NO_3 owing to decreased gas-phase NH_3 mixing ratio from reaction with SOA, as discussed in Section. 4.2 and 4.3.

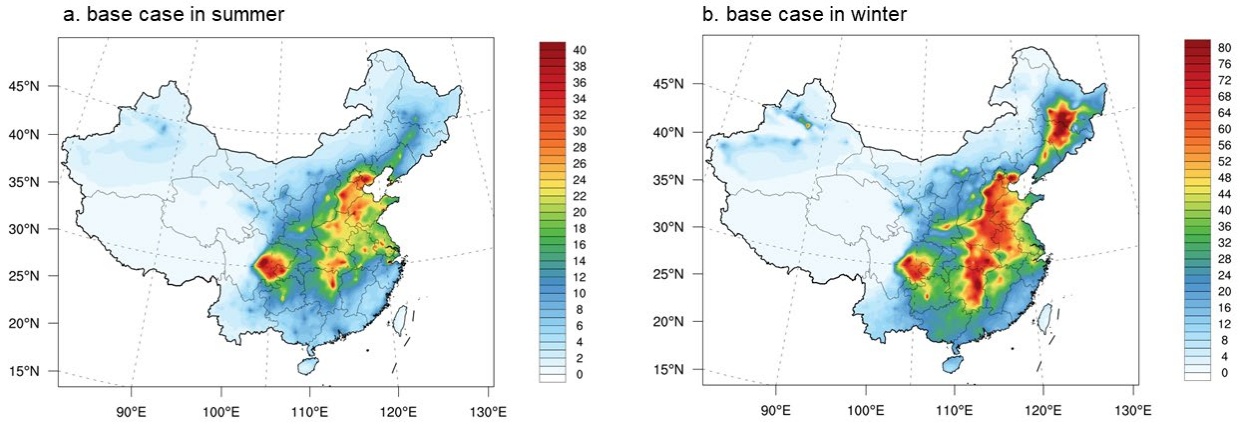

Figure 14. Spatial distribution of simulated primary and secondary $PM_{2.5}$ concentrations (unit: $\mu g\ m^{-3}$) in the base case for (a) summer and (b) winter.

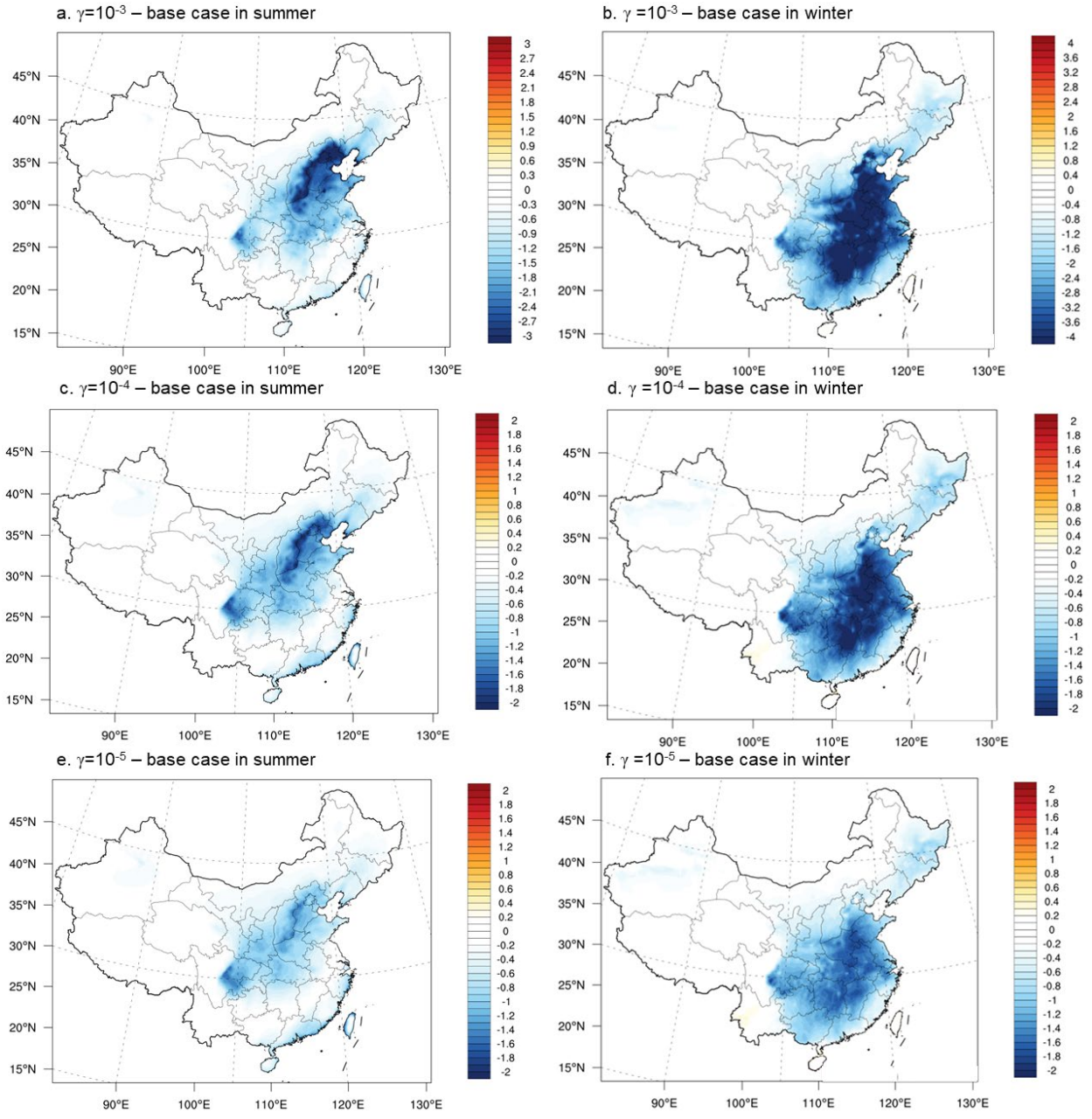

Figure 15. Spatial distribution of the difference in surface $PM_{2.5}$ concentrations (unit: μg m^{-3}) between the $\gamma = 10^{-3}$ case, $\gamma = 10^{-4}$ case, $\gamma = 10^{-5}$ case and the base case for summer and winter. Negative values represent decreases in concentration compared with the base case.

4 Conclusion

In this study, we assess the effects of the heterogeneous uptake of NH_3 by SOA accompanied by formation of NOCs on air quality over China by performing parallel simulations with a range of NH_3 uptake coefficients using the CMAQ model. The implementation of the NH_3 uptake mechanism leads to significant reductions in NH_3 mixing ratio, NH_4^+, and NO_3^- concentrations, but has little impact on SO_4^{2-} levels.

For NH_3, the reduction magnitude can be as high as 27.5% in summer and 19.0% in winter after applying the NH_3 uptake mechanism. The reduction in NH_3 results in increases in gas-phase HNO_3 concentrations, as there is less NH_3 to neutralize HNO_3 to ammonium nitrate. The increase of HNO_3 concentrations is as high as 5.7% and 9.3% in the summer and winter, respectively. Spatially, the largest decrease of NH_3 mixing ratio occurred over the North China Plain and the Sichuan Basin in both seasons. In summer, the HNO_3 increased substantially in the North China Plain, while in winter HNO_3 increased dramatically over eastern and central China. The decreases in NH_3 and increases in HNO_3 were associated with decreases in both particulate NH_4NO_3 and the total $PM_{2.5}$ in both seasons. Under the largest uptake coefficients ($\gamma = 10^{-3}$), the reduction of NH_4^+, NO_3^- and $PM_{2.5}$ concentrations in winter are 13.8%, 15.0%, and 8.7%, respectively. Larger decreases occur in summer, with reduction of 20.0%, 29.7%, and 8.9% for NH_4^+, NO_3^- and $PM_{2.5}$, respectively when $\gamma = 10^{-3}$. The impacts of NH_3 uptake on SOA concentrations, which can result from changes in particle acidity, is relatively small compared to the changes in ammonium nitrate; this is because the changes to particle acidity are relatively moderate.

Results of this study present that the mechanism of NH_3 uptake by SOA have significant impacts on HNO_3 and inorganic aerosol species including NH_3, NH_4^+, NO_3^- which further affect $PM_{2.5}$ concentrations. The results from this study are useful for understanding the potential impacts of NH_3 uptake by SOA on air quality over China. However, even though the potential impacts indicate the importance of this mechanism in air quality models, the real uptake coefficient of each SOA species may differ from the uptake coefficient used in this study which

requires further laboratory experiments for better representing the NH_3 uptake process by SOA. Additional work is also needed to develop phase separation mechanisms for improving the assumption used in this study that the aerosol had a single phase for both organic and inorganic constituents. Besides, the SOA is assumed to be well-mixed in this study then a shell of reacted SOA does not build up at the particle surface whereas this assumption may change due to the variation of the particle viscosity. Therefore, additional investigation of the possibility that a shell of reacted SOA could build up for particles with low viscosity under the condition of low relative humidity are needed in order to obtain more accurate NH_3 uptake process in numerical models. Given the uncertainty introduced by above factors, coordinated community participation is urgently needed to address these uncertainties.

Acknowledgments and Data

The authors acknowledge the MEIC team from Tsinghua University for providing the multiscale emission inventory of China (MEIC). This work was funded by the Project of Science and Technology Plan of Sichuan Province (No.2018SZDZX0023, No.2018JY0011), the National Key Research and Development Program of China (No.2018YFC0214002), the National Natural Science Foundation of China (No.91644226) and the Scientific Research Foundation of the Chengdu University of Information Technology (No.KYTZ201823). This publication was developed under Assistance Agreement No. EPA 83588101 was awarded by the US Environmental Protection Agency to the Regents of the University of California. It has not been formally reviewed by the EPA. The views expressed in this document are solely those of the authors and do not necessarily reflect those of the agency. The EPA does not endorse any products or commercial services mentioned in this publication. Any opinions, findings, and conclusions or recommendations expressed in this material are those of the authors and do not necessarily reflect the views of the funders. The authors declare no competing interests. The data presented herein are available at http://dx.doi.org/10.17632/bf8mmw9sfz.1. And the FNL analysis data are available at https://rda.ucar.edu/datasets/ds083.2.

References

Baek, B. H., Aneja, V. P., & Tong, Q. (2004). Chemical coupling between ammonia, acid gases, and fine particles. *Environmental Pollution, 129*(1), 89-98. http://www.sciencedirect.com/science/article/pii/S0269749103003816

Bai, Z., Ma, W., Ma, L., Velthof, G. L., Wei, Z., Havlík, P., et al. (2018). China's livestock transition: Driving forces, impacts, and consequences. *Science Advances, 4*(7), eaar8534. http://advances.sciencemag.org/content/4/7/eaar8534.abstract

Behera, S. N., Sharma, M., Aneja, V. P., & Balasubramanian, R. (2013). Ammonia in the atmosphere: a review on emission sources, atmospheric chemistry and deposition on terrestrial bodies. *Environmental Science and Pollution Research, 20*(11), 8092-8131. https://doi.org/10.1007/s11356-013-2051-9

Binkowski, F. S., & Roselle, S. J. (2003). Models-3 Community Multiscale Air Quality (CMAQ) model aerosol component 1. Model description. *Journal of Geophysical Research: Atmospheres, 108*(D6). https://doi.org/10.1029/2001JD001409

Byun, D., & Schere, K. L. (2006). Review of the Governing Equations, Computational Algorithms, and Other Components of the Models-3 Community Multiscale Air Quality (CMAQ) Modeling System. *Applied Mechanics Reviews, 59*(2), 51-77. https://doi.org/10.1115/1.2128636

Chen, S., Cheng, M., Guo, Z., Xu, W., Du, X., & Li, Y. (2020). Enhanced atmospheric ammonia (NH3) pollution in China from 2008 to 2016: Evidence from a combination of observations and emissions. *Environmental Pollution, 263*, 114421. http://www.sciencedirect.com/science/article/pii/S0269749119343933

Chen, Z., Xie, X., Cai, J., Chen, D., Gao, B., He, B., et al. (2018). Understanding meteorological influences on PM2.5 concentrations across China: a temporal and spatial perspective. *Atmos. Chem. Phys., 18*(8), 5343-5358. https://acp.copernicus.org/articles/18/5343/2018/

Cheng, J., Su, J., Cui, T., Li, X., Dong, X., Sun, F., et al. (2019). Dominant role of emission reduction in PM2.5 air quality improvement in Beijing during 2013–2017: a model-based decomposition analysis. *Atmos. Chem. Phys., 19*(9), 6125-6146. https://acp.copernicus.org/articles/19/6125/2019/

Fu, X., Wang, T., Gao, J., Wang, P., Liu, Y., Wang, S., et al. (2020). Persistent Heavy Winter Nitrate Pollution Driven by Increased Photochemical Oxidants in Northern China. *Environmental Science & Technology, 54*(7), 3881-3889. https://doi.org/10.1021/acs.est.9b07248

Gao, Z., Ma, W., Zhu, G., & Roelcke, M. (2013). Estimating farm-gate ammonia emissions from major animal production systems in China. *Atmospheric Environment, 79*, 20-28. http://www.sciencedirect.com/science/article/pii/S1352231013004810

Gu, B., Ju, X., Chang, J., Ge, Y., & Vitousek, P. M. (2015). Integrated reactive nitrogen budgets and future trends in China. *Proceedings of the National Academy of Sciences, 112*(28), 8792. http://www.pnas.org/content/112/28/8792.abstract

Guenther, A. B., Jiang, X., Heald, C. L., Sakulyanontvittaya, T., Duhl, T., Emmons, L. K., & Wang, X. (2012). The Model of Emissions of Gases and Aerosols from Nature version 2.1 (MEGAN2.1): an extended and updated framework for modeling biogenic emissions. *Geosci. Model Dev., 5*(6), 1471-1492. https://www.geosci-model-dev.net/5/1471/2012/

Guo, H., Otjes, R., Schlag, P., Kiendler-Scharr, A., Nenes, A., & Weber, R. J. (2018). Effectiveness of ammonia reduction on control of fine particle nitrate. *Atmos. Chem. Phys., 18*(16), 12241-12256. https://www.atmos-chem-phys.net/18/12241/2018/

Heald, C. L., Collett Jr, J. L., Lee, T., Benedict, K. B., Schwandner, F. M., Li, Y., et al. (2012). Atmospheric ammonia and particulate inorganic nitrogen over the United States. *Atmos. Chem. Phys., 12*(21), 10295-10312. https://www.atmos-chem-phys.net/12/10295/2012/

Hu, J., Chen, J., Ying, Q., & Zhang, H. (2016). One-year simulation of ozone and particulate matter in China using WRF/CMAQ modeling system. *Atmos. Chem. Phys., 16*(16), 10333-10350. https://www.atmos-chem-phys.net/16/10333/2016/

Jimenez, J. L., Canagaratna, M. R., Donahue, N. M., Prevot, A. S. H., Zhang, Q., Kroll, J. H., et al. (2009). Evolution of Organic Aerosols in the Atmosphere. *Science, 326*(5959), 1525. http://science.sciencemag.org/content/326/5959/1525.abstract

Kong, L., Tang, X., Zhu, J., Wang, Z., Pan, Y., Wu, H., et al. (2019). Improved Inversion of Monthly Ammonia Emissions in China Based on the Chinese Ammonia Monitoring Network and Ensemble Kalman Filter. *Environmental Science & Technology, 53*(21), 12529-12538. https://doi.org/10.1021/acs.est.9b02701

Li, M., Liu, H., Geng, G., Hong, C., Liu, F., Song, Y., et al. (2017). Anthropogenic emission inventories in China: a review. *National Science Review, 4*(6), 834-866. https://doi.org/10.1093/nsr/nwx150

Li, X., Ma, Y., Wang, Y., Liu, N., & Hong, Y. (2017). Temporal and spatial analyses of particulate matter (PM10 and PM2.5) and its relationship with meteorological parameters over an urban city in northeast China. *Atmospheric Research, 198*, 185-193. http://www.sciencedirect.com/science/article/pii/S0169809516303180

Li, Y., Schichtel, B. A., Walker, J. T., Schwede, D. B., Chen, X., Lehmann, C. M. B., et al. (2016). Increasing importance of deposition of reduced nitrogen in the United States. *Proceedings of the National Academy of Sciences, 113*(21), 5874. http://www.pnas.org/content/113/21/5874.abstract

Liao, T., Gui, K., Jiang, W., Wang, S., Wang, B., Zeng, Z., et al. (2018). Air stagnation and its impact on air quality during winter in Sichuan and Chongqing, southwestern China. *Science of The Total Environment, 635*, 576-585. http://www.sciencedirect.com/science/article/pii/S0048969718312920

Liu, L., Zhang, X., Xu, W., Liu, X., Li, Y., Lu, X., et al. (2017). Temporal characteristics of atmospheric ammonia and nitrogen dioxide over China based on emission data, satellite observations and atmospheric transport modeling since 1980. *Atmos. Chem. Phys., 17*(15), 9365-9378. https://www.atmos-chem-phys.net/17/9365/2017/

Liu, Y., Liggio, J., Staebler, R., & Li, S. M. (2015). Reactive uptake of ammonia to secondary organic aerosols: kinetics of organonitrogen formation. *Atmos. Chem. Phys., 15*(23), 13569-13584. https://www.atmos-chem-phys.net/15/13569/2015/

Meng, Z., Xu, X., Lin, W., Ge, B., Xie, Y., Song, B., et al. (2018). Role of ambient ammonia in particulate ammonium formation at a rural site in the North China Plain. *Atmos. Chem. Phys., 18*(1), 167-184. https://www.atmos-chem-phys.net/18/167/2018/

Montoya-Aguilera, J., Hinks, M. L., Aiona, P. K., Wingen, L. M., Horne, J. R., Zhu, S., et al. (2018). Reactive Uptake of Ammonia by Biogenic and Anthropogenic Organic Aerosols. In *Multiphase Environmental Chemistry in the Atmosphere* (Vol. 1299, pp. 127-147): American Chemical Society.

Pan, Y., Tian, S., Zhao, Y., Zhang, L., Zhu, X., Gao, J., et al. (2018). Identifying Ammonia Hotspots in China Using a National Observation Network. *Environmental Science & Technology, 52*(7), 3926-3934. https://doi.org/10.1021/acs.est.7b05235

Paulot, F., Jacob, D. J., Pinder, R. W., Bash, J. O., Travis, K., & Henze, D. K. (2014). Ammonia emissions in the United States, European Union, and China derived by high-resolution inversion of ammonium wet deposition data: Interpretation with a new agricultural emissions inventory (MASAGE_NH3). *Journal of Geophysical Research: Atmospheres, 119*(7), 4343-4364. https://doi.org/10.1002/2013JD021130

Pye, H. O. T., Pinder, R. W., Piletic, I. R., Xie, Y., Capps, S. L., Lin, Y.-H., et al. (2013). Epoxide Pathways Improve Model Predictions of Isoprene Markers and Reveal Key Role of Acidity in Aerosol Formation. *Environmental Science & Technology, 47*(19), 11056-11064. https://doi.org/10.1021/es402106h

Qin, M., Wang, X., Hu, Y., Ding, X., Song, Y., Li, M., et al. (2018). Simulating Biogenic Secondary Organic Aerosol During Summertime in China. *Journal of Geophysical Research: Atmospheres, 123*(19), 11,100-111,119. https://doi.org/10.1029/2018JD029185

Reiss, R., Anderson, E. L., Cross, C. E., Hidy, G., Hoel, D., McClellan, R., & Moolgavkar, S. (2007). Evidence of Health Impacts of Sulfate-and Nitrate-Containing Particles in Ambient Air. *Inhalation Toxicology, 19*(5), 419-449. https://doi.org/10.1080/08958370601174941

Sun, Y., Chen, C., Zhang, Y., Xu, W., Zhou, L., Cheng, X., et al. (2016). Rapid formation and evolution of an extreme haze episode in Northern China during winter 2015. *Scientific Reports, 6*(1), 27151. https://doi.org/10.1038/srep27151

Updyke, K. M., Nguyen, T. B., & Nizkorodov, S. A. (2012). Formation of brown carbon via reactions of ammonia with secondary organic aerosols from biogenic and anthropogenic precursors. *Atmospheric Environment, 63*, 22-31. http://www.sciencedirect.com/science/article/pii/S1352231012008710

Walters, W. W., Chai, J., & Hastings, M. G. (2019). Theoretical Phase Resolved Ammonia–Ammonium Nitrogen Equilibrium Isotope Exchange Fractionations: Applications for Tracking Atmospheric Ammonia Gas-to-Particle Conversion. *ACS Earth and Space Chemistry, 3*(1), 79-89. https://doi.org/10.1021/acsearthspacechem.8b00140

Wang, P., Ying, Q., Zhang, H., Hu, J., Lin, Y., & Mao, H. (2018). Source apportionment of secondary organic aerosol in China using a regional source-oriented chemical transport model and two emission inventories. *Environmental Pollution, 237*, 756-766. http://www.sciencedirect.com/science/article/pii/S0269749117324065

Weber, R. J., Guo, H., Russell, A. G., & Nenes, A. (2016). High aerosol acidity despite declining atmospheric sulfate concentrations over the past 15 years. *Nature Geoscience, 9*(4), 282-285. https://doi.org/10.1038/ngeo2665

Wu, K., Yang, X., Chen, D., Gu, S., Lu, Y., Jiang, Q., et al. (2020). Estimation of biogenic VOC emissions and their corresponding impact on ozone and secondary organic aerosol formation in China. *Atmospheric Research, 231*, 104656. http://www.sciencedirect.com/science/article/pii/S0169809519304715

Yang, X., Lu, Y., Zhu, X., He, J., Jiang, Q., Wu, K., et al. (2020). Formation and Evolution Mechanisms of Severe Haze Pollution in the Sichuan Basin, Southwest China. *Aerosol and Air Quality Research, 20*(11), 2557-2567. http://dx.doi.org/10.4209/aaqr.2020.04.0173

Zhang, H., Cheng, S., Li, J., Yao, S., & Wang, X. (2019). Investigating the aerosol mass and chemical components characteristics and feedback effects on the meteorological factors

715 in the Beijing-Tianjin-Hebei region, China. *Environmental Pollution, 244*, 495-502.
716 https://www.sciencedirect.com/science/article/pii/S0269749118325910
717 Zhang, L., Chen, Y., Zhao, Y., Henze, D. K., Zhu, L., Song, Y., et al. (2018). Agricultural
718 ammonia emissions in China: reconciling bottom-up and top-down estimates. *Atmos.*
719 *Chem. Phys., 18*(1), 339-355. https://www.atmos-chem-phys.net/18/339/2018/
720 Zhang, Q., Pan, Y., He, Y., Zhao, Y., Zhu, L., Zhang, X., et al. (2019). Bias in ammonia
721 emission inventory and implications on emission control of nitrogen oxides over North
722 China Plain. *Atmospheric Environment, 214*, 116869.
723 https://www.sciencedirect.com/science/article/pii/S1352231019304996
724 Zhang, Y., Ding, A., Mao, H., Nie, W., Zhou, D., Liu, L., et al. (2016). Impact of synoptic
725 weather patterns and inter-decadal climate variability on air quality in the North China
726 Plain during 1980–2013. *Atmospheric Environment, 124*, 119-128.
727 https://www.sciencedirect.com/science/article/pii/S1352231015301345
728 Zheng, B., Tong, D., Li, M., Liu, F., Hong, C., Geng, G., et al. (2018). Trends in China's
729 anthropogenic emissions since 2010 as the consequence of clean air actions. *Atmos.*
730 *Chem. Phys., 18*(19), 14095-14111. https://www.atmos-chem-phys.net/18/14095/2018/
731 Zheng, B., Zhang, Q., Zhang, Y., He, K. B., Wang, K., Zheng, G. J., et al. (2015). Heterogeneous
732 chemistry: a mechanism missing in current models to explain secondary inorganic
733 aerosol formation during the January 2013 haze episode in North China. *Atmos. Chem.*
734 *Phys., 15*(4), 2031-2049. https://www.atmos-chem-phys.net/15/2031/2015/
735 Zheng, G. J., Duan, F. K., Su, H., Ma, Y. L., Cheng, Y., Zheng, B., et al. (2015). Exploring the
736 severe winter haze in Beijing: the impact of synoptic weather, regional transport and
737 heterogeneous reactions. *Atmos. Chem. Phys., 15*(6), 2969-2983. https://www.atmos-
738 chem-phys.net/15/2969/2015/
739 Zhu, L., Henze, D. K., Bash, J. O., Cady-Pereira, K. E., Shephard, M. W., Luo, M., & Capps, S.
740 L. (2015). Sources and Impacts of Atmospheric NH3: Current Understanding and
741 Frontiers for Modeling, Measurements, and Remote Sensing in North America. *Current*
742 *Pollution Reports, 1*(2), 95-116. https://doi.org/10.1007/s40726-015-0010-4
743 Zhu, S., Horne, J. R., Montoya-Aguilera, J., Hinks, M. L., Nizkorodov, S. A., & Dabdub, D.
744 (2018). Modeling reactive ammonia uptake by secondary organic aerosol in CMAQ:
745 application to the continental US. *Atmos. Chem. Phys., 18*(5), 3641-3657.
746 https://www.atmos-chem-phys.net/18/3641/2018/

747

Journal of Geophysical Research: Atmospheres

Supporting Information for

Modeling ammonia and its uptake by secondary organic aerosol over China

Kai Wu[1,2], Shupeng Zhu[2,3*], Yiming Liu[4,5], Haolin Wang[4,5], Xianyu Yang[6], Lei Liu[7], Donald Dabdub[3], Christopher D. Cappa[8*]

[1]Department of Land, Air, and Water Resources, University of California, Davis, CA, USA

[2]Advanced Power and Energy Program, University of California, Irvine, CA, USA

[3]Computational Environmental Sciences Laboratory, Department of Mechanical and Aerospace Engineering, University of California, Irvine, CA, USA

[4]School of Atmospheric Sciences, Sun Yat-sen University, Zhuhai, China

[5]Guangdong Provincial Observation and Research Station for Climate Environment and Air Quality Change in the Pearl River Estuary, Key Laboratory of Tropical Atmosphere-Ocean System, Ministry of Education, Southern Marine Science and Engineering Guangdong Laboratory (Zhuhai), Zhuhai, China

[6]Plateau Atmosphere and Environment Key Laboratory of Sichuan Province, School of Atmospheric Sciences, Chengdu University of Information Technology, Chengdu, China

[7]College of Earth and Environmental Sciences, Lanzhou University, Lanzhou, China

[8]Department of Civil and Environmental Engineering, University of California, Davis, CA, USA

Contents of this file

Introduction

Figure S1 displays the model domain with important regions colored over China. Figure S2 shows the spatial distribution of allocated emission of NO_2 and SO_2 in the summer of 2017 over China. Figure S3 presents the spatial distribution of the particle pH in the base case for summer and winter.

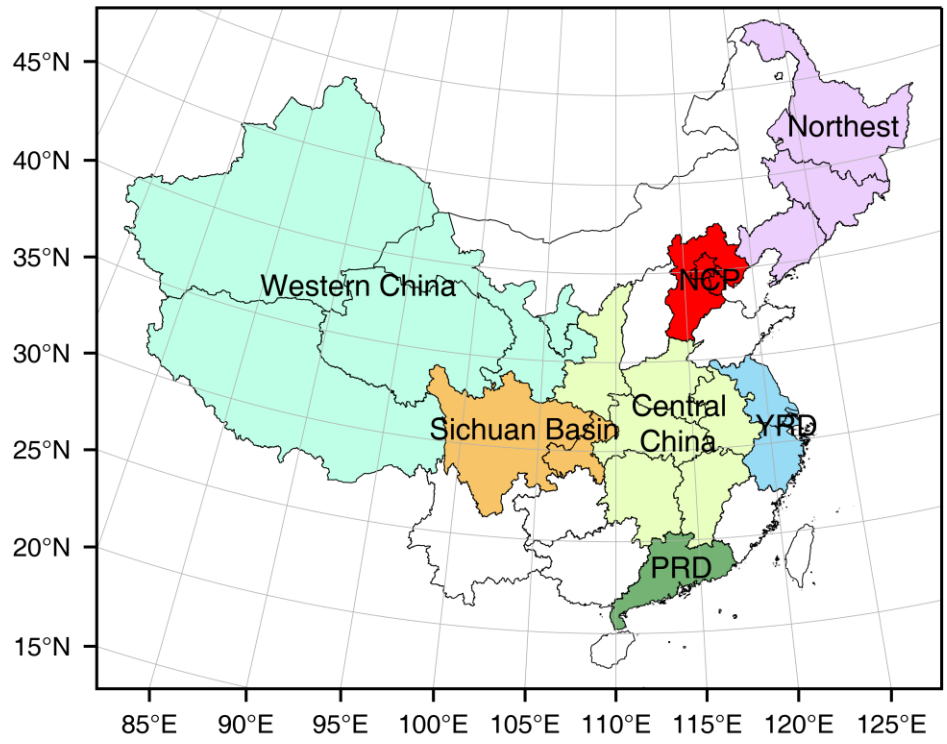

Figure S1. Model domain with important regions colored over China.

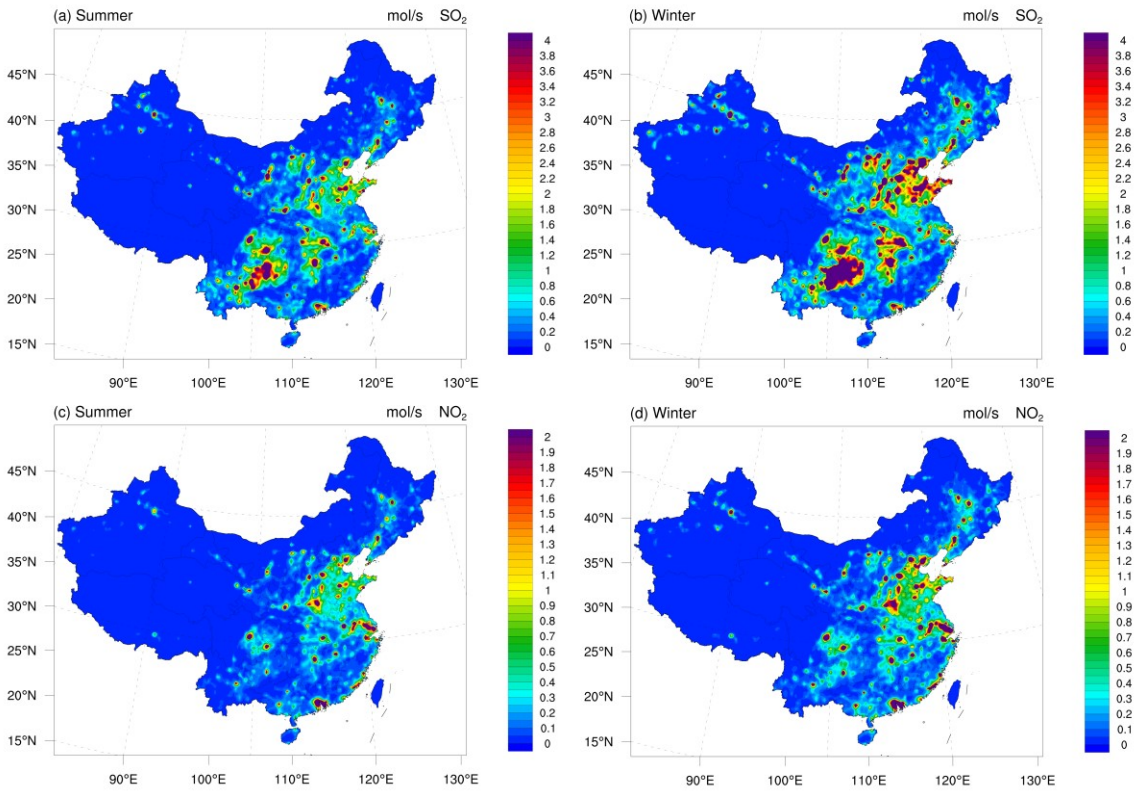

Figure S2. Spatial distribution of allocated emission rate of NO_2 and SO_2 in the summer and winter of 2017 over China.

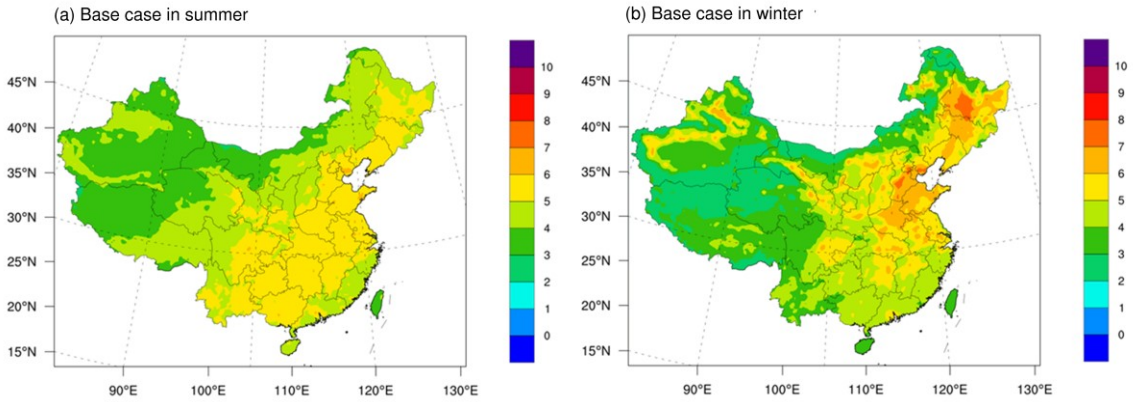

Figure S3. Spatial distribution of the particle pH in the base case for summer and winter.